Ultralow noise pre-amplified receiver for free-space optical communications

Ravikiran Kakarla

Photonics Laboratory
Department of Microtechnology and Nanoscience
Chalmers University of Technology
Gothenburg, Sweden, 2020

Front cover illustration: A graph of sensitivities achieved by various receivers including PSA pre-amplified receiver.

Ultralow noise pre-amplified receiver for free-space optical communications

Ravikiran Kakarla

Photonics Laboratory

Department of Microtechnology and Nanoscience

Chalmers University of Technology

Abstract

The demand for high data rate in space communication links is increasing due to the growth of space exploration missions inter-satellite, and satellite-to-Earth data transmission. Optical communication systems capable of handling hundreds of Gigabits per second data transmission with a single light carrier and are suitable for such space links. In addition, light offers smaller beam divergence in space due to the shorter wavelength compared to radio frequency beams (RF), resulting in smaller link loss and smaller size receiver apertures required.

The receiver sensitivity is one of the key factors that determines the capacity and reach for such long haul communication links. Currently, there is a search for the optimal modulation format and receiver implementation combination to achieve the best sensitivity for error-free transmission. In this thesis, we discuss and implement the best possible combination of these, both theoretically and experimentally.

Phase sensitive parametric optical amplifier (PSA) can amplify optical signals ideally without adding any excess noise, limited only by quantum fluctuations. Employing these as pre amplifiers in free-space receivers can thus improve the sensitivity compared to erbium doped fiber amplifiers. We implement a two-mode PSA with a noise figure of 1.2 dB, which can amplify both quadratures of a signal, being used as a pre-amplifier in coherent receiver setup. We experimentally demonstrate a record "black-box" sensitivity of 1 photon-per-bit using PSA receiver for quadrature phase shift keying (QPSK) modulation format at 10.5 Gbps with 100 % overhead forward error correction code. This sensitivity also includes ultra-low pump power (-72 dBm) which is recovered using pre-amplified injection locking.

We also investigate the most power efficient modulation formats, where a combination of m-(pulse-position modulation) PPM+QPSK with higher m-values provides best sensitivity at relatively high received SNR-per-bit, while QPSK outperforms all formats investigated at very low SNR-per-bit, which is ideal for space communications.

Keywords: Phase sensitive amplifier, optical injection locking, sensitivity, and noise figure

Publications

This thesis is based on the work contained in the following papers:

[A] R. Kakarla, K. Vijayan, A. Lorences-Riesgo, P.A. Andrekson, "High Sensitivity Receiver Demonstration Using Phase Sensitive Amplifier for Free-Space Optical Communication", *Proceedings of European Conference on Optical Communications(ECOC)*, Paper. Tu.2.E.3, 2017.

[B] R. Kakarla, J. Schröder, and P.A. Andrekson, "Optical injection locking at sub nano-Watt powers", *Optics Letters.* vol. 43, no. 23, pp. 5769-5772, 2016.

[C] R. Kakarla, J. Schröder, and P.A. Andrekson, "Record-sensitivity Gb/s receiver for free-space applications based on phase-sensitive amplification", *Conference on Lasers and Electro-Optics (CLEO)*, pp. 1-2, 2019. (Post deadline paper).

[D] R. Kakarla, J. Schröder, and P.A. Andrekson, "One photon-per-bit receiver using near-noiseless phase-sensitive amplification", *Accepted for publication in Light: Science and Applications.*

[E] R. Kakarla, J. Schröder, and P.A. Andrekson, "Power efficient communication for high data-rate deep-space optical links", *To be submitted.*

Related papers by the author but not included in the thesis:

1. R. Kakarla, K. Vijayan, J. Schröder, P.A. Andrekson, Phase noise characteristics of injection-locked lasers operated at low injection powers, *Optical Fiber Communication Conference (OFC), OSA Technical Digest (online)*, paper M4G.2, 2018.

2. J. Schröder,R. Kakarla and P.A. Andrekson, Record-Sensitivity Receiver at 1 Photon/Bit for Free-Space Applications, *Asia Communications and Photonics Conference (ACP)*. pp. 1-3, 2019.

3. P.Zhao, R. Kakarla, M. Karlsson,, and P.A. Andrekson, Enhanced analog-optical link performance with noiseless phase-sensitive fiber-optical parametric amplifiers, *Opt. Express*, vol. 28, pp. 23534-23544, 2020.

Contents

Acknowledgement

First of all I would like to thank my supervisors Prof. Peter Andrekson, Prof. Magnus Karlsson for accepting me as a PhD student. Thanks to Prof. Peter and Dr. Jochen for supervising and motivating me all these years. Abel Lorences Riesgo deserves a special thanks for teaching me how to implement PSA experimentally and everything for the first time and guiding me to write the first paper. Thanks to Jochen Schröder for bearing with my writing and helping improve writing skills, although I am still improving. Mikael Mazur deserves a big thanks for supporting while he was here and also for all the help with the DSP in last few days, deserves my gratitude.

I would like to thank all the lab mates for all the interesting discussions, Kovendhan Vijayan for all discussions on PSAs and all lab stuff, Ali Mirani for sharing his knowledge on information theory and also his codes. Although I am not big sports guy, I also played some sports, which I realized is most important to stay activem credit to Kovendhan. I would like to thank all ping-pong mates, for showing me some good competition, Kovendhan, Ali, Krishna, Mehdi and many more. I would like thank my friend Ayesha for sharing all the interesting stuff. Finally my family, sister, mom and dad for their care and good suggestions all the time.

<div align="right">Ravikiran Kakarla</div>

x

Acronyms

APD	Avalanche photo detector
ASE	Amplified spontaneous emission
AWGN	Additive white gaussian noise
BPSK	Binary phase shift keying
BCH	BoseâChaudhuriâHocquenghem codes
DFB	Distributed feedback laser
DQ	Dual quadrature
EDFA	Erbium doped fiber amplifier
FEC	Forward error correction
FSK	Frequency shift keying
FWM	Four-wave mixing
GEO	Geostationary orbit
HD	High definition
HNLF	Highly nonlinear fiber
ILIP	Injection locking induced pulsations
LDPC	Low density parity check codes
LLCD	Lunar laser communication demonstration
LRCD	Laser relay communication demonstration
LO	Local oscillator
NASA	National Aeronautics and Space Administration
NF	Noise figure
OIL	Optical injection locking
OSNR	Optical signal to noise ratio
PLL	Phase locked loop
PMT	Photomultiplier tube
PPB	Photons-per-bit
PPM	Pulse position modulation
PSA	Phase sensitive amplification
PSA	Power spectral density
PZT	Piezoelectric transducer
PS-QPSK	Polarisation switched quadrature phase shift keying

QPSK	Quadrature phase shift keying
RF	Radio frequency
SNR	Signal to noise ratio
SNSPD	Superconducting nanowire single photon detector
SN	Shot noise
SQ	Single quadrature
SOP	State of polarisation
WDM	Wavelength division multiplexing

Chapter 1

Introduction

Future expeditions into deep-space require fast and efficient ways of communication with earth. The demand for returning larger data volumes from deep space missions is continuously growing to support high resolution instruments for real-time data transfer, space exploration of humans and to practice a virtual presence by high definition (HD) videos or images. Due to these high data rate demanding applications, radio frequency (RF) communications needs to perform 100 fold faster and more efficient than today [1, 2]. Current state-of-the-art RF communication systems for deep-space network operate in the Ka-band frequencies (26 GHz - 40 GHz) having replaced previous generation X-band frequencies (1 - 10 GHz) for space missions such as Mars Reconnaissance orbiter (MRO) 2005, Cassini at Saturn, 2004 [2].

The challenging aspect of long distance deep-space communication is their extremely low received powers due to the divergence of the beam, which induces significant loss due to the aperture size. Thus in RF communications for deep-space links, antenna sizes on the ground used for deep-space network (DSN) are extremely large, typically between 30 m to 70 m in diameter [3]. The increase in distance of communication reduces the received power, also results in lowered data-rates. For example, systems that can transmit 10 Gbps data from GEO orbit to ground station may only achieve 10 bps from Saturn situated at 1 billion kilometres from Earth [1]. The only way to communicate at higher data rates is to increase either transmitted power or receiver sensitivity. Increasing the receiver sensitivity can be possible by choosing appropriate modulation formats, forward error codes (FEC) and high sensitive receivers [1]. In RF deep-space communications, the achieved nominal data rates were upto 6 Mbps to Mars in Mars reconnaissance orbiter (MRO) 2006 and few hundred kbps to Saturn in Cassini 2004 [1].

Ever since the discovery of the laser in the early 1960s, the use of light for communications have been pursued. Since that time, advances in lasers,
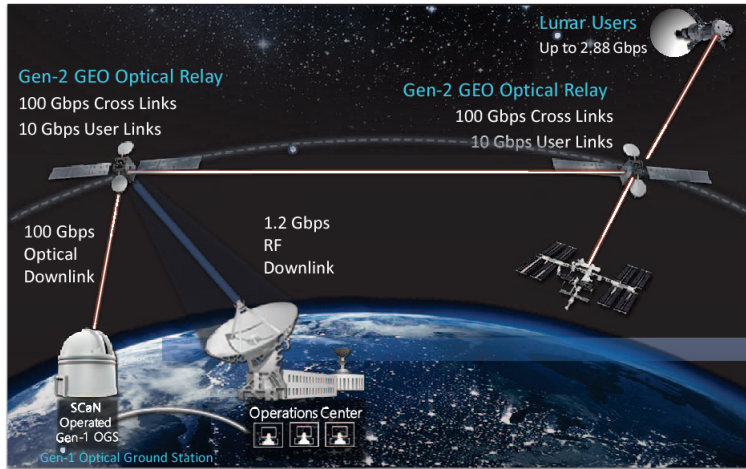
Figure 1.1: NASA relay constellation in 2025 [11]

detectors and optics have resulted in a number of successful demonstrations of free-space communications. These include Orbit-to-Orbit and Orbit-to-ground links [4–8]. The higher carrier frequency (10^4 times) and lower beam divergence makes light an important medium for space communications to achieve high data rates as well as longer reach.

NASA's lunar laser communication demonstration (LLCD) was the first attempt to optically reach deep-space, with a laser based transceiver on a satellite orbiting the moon operating at 1550 nm wavelength achieving a down-link with 622 Mbps rate to Earth [9]. This demonstration in 2013 paved the way to upcoming missions include laser communication to Mars by 2022 [10] and high speed near earth communication such as laser communication relay demonstration (LRCD) for downloading multi-tera bytes of data per day from outer space satellites as well as high speed communication within the relay network in GEO and ground station as shown in Fig. 1.1 [11]. Along side these, space missions involving human travel is the 'Orion EM-2' optical communication terminal, where the objective is to provide bi-directional multi purpose crew vehicle in the lunar vicinity, sending humans to space and communicating using lasers at initial targeted speeds of 250 Mbps and later increase to Gbps speeds [12]. Many upcoming missions intended to probe into space are likely to use optical communications operating at multi Gbps data rates.

Optical beams exhibit lower beam divergence compared to RF beams, as beam divergence angle is proportional to wavelength allowing optical beams to be 10^4 times narrower than RF beams. This means more power is concentrated in a smaller area allowing the laser communication to be power efficient than

RF communication and result in smaller dimensions of the receiver antennas or detectors. This puts a stringent requirement on precise beam alignment which was accomplished in LLCD 2013 [13]. Large receiver aperture in optical communication can be emulated by multiple small apertures and combining them coherently instead of using a large size antenna [14, 15].

Optical transmitters and receivers are widely available in the C-band (1530 - 1560 nm) and L-band (1560 -1625 nm) due to well established fiber-optic communication technology. These power efficient transmitter and receiver technologies can be adapted from fiber-optic technology. Typical power efficient modulation formats that are used in free-space communication are Pulse position modulation (PPM), polarisation switching cascaded with QPSK or higher order QAM [16], frequency shift keying (FSK) has been demonstrated in [17,18] along with high sensitive optical receivers or detectors. The most widely used approach is pulse position modulation along with direct detection optical receivers such as super conducting nano-wire single photon detectors (SN-SPDs), single photon avalanche photodetectors (APDs). [19–21]. The drawback with such detectors is their available limited bandwidth of few GHz, which imposes restriction on the achievable data rates. Moreover by using power efficient modulation formats such as PPM, the achieved data rates can be much less than the detection bandwidths, which are limited to few Mbps.

Coherent detection and spectral efficient modulation formats are therefore of importance for future communication links operating at Gbps data rates. However, power efficiency is one important factor that should be considered along with spectral efficiency. Power efficient modulation formats with coherent detection are polarisation switched(PS)-QPSK, or PPM+QPSK which combining PPM and QPSK to achieve better sensitivity. On the receiver side, coherent homodyne receivers are theoretically optimal as they provide the best capacity of all receivers while their low detection quantum efficiency can limit the practical performance. Pre-amplified receivers can also be used to improve the receiver sensitivity. Typically erbium doped fiber amplifiers (EDFA) are used as pre-amplifiers having a ideal noise figure (NF) of 3 dB which results in a degradation of the signal to noise ratio(SNR) by a factor of 2. Phase sensitive amplifiers (PSA) can ideally have a NF of 0 dB [22], employing such a pre-amplifier can provide noise free detection of one or both quadratures of the optical signal. Single quadrature phase sensitive amplifiers demonstrated [23] in the context of phase regeneration by squeezing the noise in one dimension, can be used as a noise free amplifier for single quadrature signal such as binary phase shift keyed signal (BPSK). Although this is a great demonstration, the technique can only amplify single quadrature of the signal, which is not spectrally efficient as another quadrature of the signal is not being used.

A two mode PSA [24], can amplify both quadratures of the signal noise-free, where it needs two waves, the signal and the idler at input of the PSA to perform noise-free amplification in both quadratures of light. The two mode PSA

has same spectral efficiency as that of single mode PSA, allowing noise-free detection in both quadratures to perform coherent detection of any advanced modulation format. If implemented using a fiber-optic parametric amplification [25] where the signal and idler waves are simultaneously amplified using parametric amplification and coherently combined to achieve phase sensitive amplification. Strained highly non-linear fibers (HNLFs) are typically used achieving parametric amplification with maximum gain, demonstrated in [26].

1.1 This work

In this work, we demonstrate a phase sensitive parametric amplifier as a pre-amplifier in a free-space communication scenario at extremely low received power levels.

In Paper(A), we demonstrated the feasibility of a phase sensitive amplified receiver for a free-space channel, i.e atmospheric channel as well as deep space channel. The atmospheric channel is emulated in the laboratory with a rotating turbulence phase screen plate, designed to introduce turbulence effects on the incident light beam. We studied the effect of turbulence on all the waves in free-space channel on phase sensitive amplifier and the corresponding sensitivity and compared against the performance against a non-atmospheric channel.

In Paper(B), Unlike EDFA, PSAs require additional waves at the input, signal, idler (conjugate of signal) and the pump wave. The pump power is transmitted to be much lower than signal and idler to minimize the penalty. Such a lower power pump typically below -65 dBm and is recovered using optical injection locking (OIL) supported by a phase locked loop. We discuss in detail the implementation of stable pump regeneration by optical injection locking at -65 dBm using a PLL and a pre-amplifier. We investigate the inherent phase noise generated due to low injected powers in injection locking and discuss its implications on the performance of a phase sensitive amplifier. We gave a theoretical explanation for why phase noise increases at low injected powers and proved experimentally.

In paper (C), we demonstrated a sensitivity of 1 photon per bit using a phase sensitive amplified receiver for free-space communication where we use QPSK modulation and standard forward error correction with 100 percent overhead.

In paper (D), we improve the results of paper (c) and show a black box error-free sensitivity of 1 photon per bit of the PSA pre-amplified receiver for a transmitted QPSK data at 10 Gbps rate. We derive the expressions for theoretical sensitivity achieved using PSA coherent receiver and compared with most of the receivers used for free-space or deep-space communications.

In paper (E), we show the best modulation format for high sensitivity communication where we combine PPM with QPSK to achieve improved power efficiency. However, simple QPSK can outperform all formats at low SNR per

bit regime. We experimentally demonstrate all performance of all these formats with PSA receiver and calculate their sensitivities.

This thesis is organized as follows. Chapter 2 introduces with different types of free-space communication channels and their impairments for a link with PSA based receiver and a regular link. In Chapter-3, the theory of the fiber-optic parametric amplification and phase sensitive amplification in non-linear fibers is discussed. Chapter-4 discusses systems level components used in free-space communication/ deep-space communications for high power efficiency in particular. Power efficient modulation formats, detectors/ receivers and also the corresponding achievable information rates of using various modulation formats/ detection schemes are discussed. Overall implementation challenges of practical phase sensitive amplifiers for free-space communication are discussed in chapter 5, which involves optical injection locking, polarisation challenges, pump power optimizations and also digital signal processing challenges.

Chapter 2

Free-space optical communications

2.1 Free-space optical communication links

Free-space optical communication links are point-to-point links have been implemented as ground-to-ground, space-to-ground and space-to-space links. Communication links on Earth are typically short distance(few kilo-meters) atmospheric links supplement to RF/microwave links to establish broadband connectivity [27]. The data rates provided by these links continue to increase in both short and long range communications within atmosphere. Typical applications of these links include mobile and airborne platforms. Problems involved with long range links are the atmospheric turbulence and scintillation effects present challenges with fading and beam pointing. [28].

In deep-space links, communication takes place between a deep space satellite and a communication receiver on Earth or in orbit around Earth. The satellite in deep-space is usually the transmitter sending high speed data to the ground station or to a satellite in the orbit which serves as relay.

A schematic of a typical free-space optical communication system is shown in the Fig. (2.1).

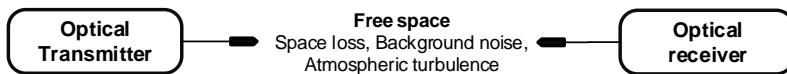The functions of the optical transmitter are to encode and modulate the

Figure 2.1: Free space communication link [1]

information onto the optical carrier, provide appropriate power by amplifying the signal and provide necessary lens arrangement to point towards the receiver.

The signal passes through the optical channel which adds loss due to the divergence of the beam, inversely proportional to the link distance z squared, $1/z^2$ [1]. The free-space channel also introduces background noise from the sun, moon and bright stars for deep-space links. If the Earth terminal is ground based, the signal passes through the Earth's atmosphere which introduces sky irradiance, scintillations due to turbulence effects and attenuation due to clouds and rain etc.

The function of the receiving terminal is to have appropriate receiver optics to receive the light with maximum efficiency and to provide sufficient sensitivity to receive signals, demodulate and decode the information [1].

2.2   Link equation and received signal power

The performance of the optical link is primarily determined by the received signal power, which is governed by the link equation [1].

$$P_s = P_t \left(\eta_T \frac{4\pi A_T}{\lambda_T^2} \right) L \left(\frac{A_R}{4\pi z^2} \right) \eta_R \qquad (2.1)$$

where
P_s, P_t are received and transmitted signal power at input to receiver and at transmit antenna interface.
η_T, η_R are the transmitting and receiving optics efficiency.
A_T, A_R are the aperture areas of transmitting and receiving optics
L is the loss in the channel due to the beam pointing inaccuracy.
z is the link distance and $A_R/4\pi z^2$ is the fraction of power collected by receiving aperture considering transmitter is isotropic.
λ_T is the wavelength of the transmitted signal. Optical carrier wavelength (frequency, $f_{optical} = 200$ THz) is much shorter compared to the RF ($f_{RF} = 20$ GHz). Hence optical beams diverges less than RF beams resulting higher received signal power (10^8 times).

According to the link equation Eq. (2.1), the received power can be increased by either:

- Increasing transmitted power, but this might lead to an excess power consumption in the space craft.

- Increasing the transmitter aperture, but size is correlated with mass which is the primary driver of cost for space missions.

- Reducing operating wavelength of signal, but lasers and detectors at such wavelengths are not necessarily available.
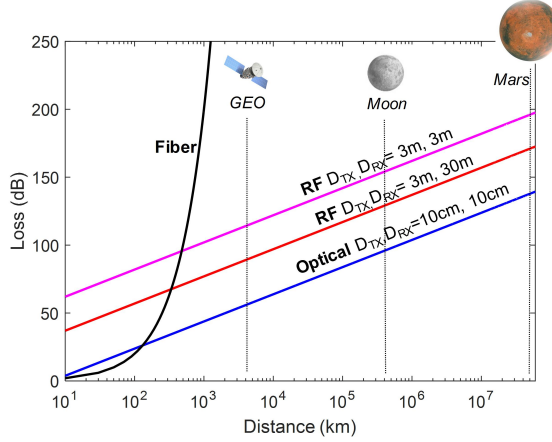
Figure 2.2: Link losses of RF and optical communications in deep space from surface of Earth

- Increasing receiver aperture area, but this can be useful when the receiver is on the ground and not with receiver on the satellite. Another drawback of this is that the amount of background noise collected also increases with receiver aperture.

The typical link losses for deep-space links using RF and optical beams were shown in Fig. 2.2. RF links used for deep-space communication, such as Mars and other planets have receiver antenna aperture size larger than 30m [3] whereas the transmitting antenna sizes are around 3 m for the satellite in space. The loss of RF links is calculated using standard free-space path loss formula [29], where the gain and size of antennas are considered according to NASA's deep-space network(DSN) antennas. The typical inter satellite links between different orbits around Earth use 3 m antennas in both transmitter and receiver. These are especially the relay satellites carrying high-speed data to Earth. On the other hand, optical link losses are calculated using Eq. (2.1) where transmitting and receiving aperture sizes are typically 10 cm [1] for all types of space links. A fiber link loss was also shown to provide an idea that exponential loss in fiber makes it impossible to communicate to such longer distances.

In the Fig. 2.2, the distance on x-axis is measured from the surface of the earth. The GEO orbit situated at 35000 Km above surface of earth will experience a 50 dB divergence loss with optical links while with RF link link it is atleast 80 dB. Note that these link losses are due to divergence of beams only. Practically, there will be additional losses due to beam pointing, coupling light into fiber etc. for optical beams.
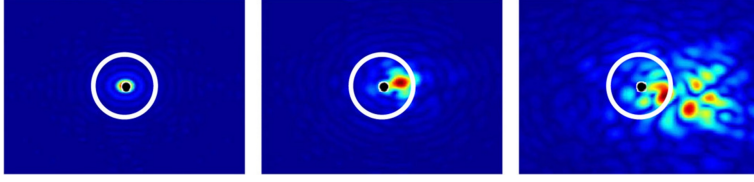
Figure 2.3: Influence of atmospheric turbulence on optical beam with increasing turbulence strength [30]

To communicate to a satellite around moon using optical links, one has to account for a link losses of atleast 80-100 dB and to Mars the losses are close to 150 dB. Satellites usually equipped with high power lasers instead of booster amplifiers to have less power consumption, where try transmit less than 1 W of power (0.5 W in the case of LLCD) only [9]. Hence receiver sensitivity is the most important metric in such links. In chapter 4, we discuss different methods to improve receiver sensitivity.

2.3 Atmospheric channel

A deep-space channel can simply be assumed as attenuation only channel whereas the atmospheric channel is affected by the turbulence and visibility, affecting the link performance [30]. Atmospheric turbulence creates beam-wandering (changing direction of the beam) and scintillations resulting in phase and amplitude fluctuations in the wave-front which obey Kolmogorov statstics of turbulence, as depicted in the Fig. 2.3 [31]. Due to the strong turbulence, the received optical beam splits into multiple small beams and also changes its direction due to the refractive index variations in the path [31, 32]. These spatial variations can convert to time varying amplitude and phase fluctuations in the received signal after the light focussed into an optical fiber. The refractive index fluctuations seen by the optical beam due to atmospheric turbulence is characterized by a parameter called atmospheric structure constant of the refractive index C_n^2, which indicates the strength of the turbulence. The spatial phase distortion of the beam due to turbulence is quantified by a parameter called Rytov variance given by the expression [31]

$$\sigma^2 = 1.23 C_n^2 (2\pi/\lambda)^{7/6} L^{11/6} \tag{2.2}$$

where L is the length in meters and λ is the wavelength. The rytov approximation predicts that the fluctuations increase monotonically with link length.

When performing experiments in a laboratory environment, real atmospheric turbulence can be emulated using a turbulence phase plate. This plate

is written with random refractive index variations around it with a variance equal to the rytov variance of the corresponding atmospheric link.

2.3.1 Turbulence phase plate

The effects of turbulence can be emulated by a rotating phase screen plate in the laboratory environment in a short distance free-space link of 1 meter distance. The random phase distribution obeying Kolmogorov statistics are characterized by an effective Fried coherence length (Spatial) r_0, was machined on the plate by Lexitec.Inc [33].

The parameter r_0 is defined as the diameter of wave front area over which the r.m.s phase variations due to turbulence equal to 1 rad. If the beam size is much larger than the r_0 value, we can consider that the effect of turbulence on the beam is minimal and vice versa.

The strength of the atmospheric turbulence is varied by varying the r_0 value or the incident optical beam size on the plate by changing the location of the plate between transmitter and receiver [34, 35]. The atmospheric structure constant for a phase plate is given by

$$C_n^2 = 2.36(\lambda/2\pi)^2(r_0)^{-5/3} \tag{2.3}$$

and the corresponding Rytov variance

$$\sigma^2 = 0.56 C_n^2 (2\pi/\lambda)^{7/6}(0.25L)^{5/6} \tag{2.4}$$

To relate the parameters of the simulated link to the real atmosphere, it is required that the Rytov varience of practical atmospheric link Eq. (2.2) should be equal to the estimated lab link Eq. (2.4) [34, 35]. The design parameter r_0 for the phase plate, describing the amount of turbulence induced within the beam is chosen to match the real atmospheric turbulence over a desired distance. [33]. In paper (A), we discuss the emulation of atmospheric turbulence using a phase plate with a r_0 values 0.3mm, 0.8mm and 2mm for high, medium and low turbulence for a 1 km real atmospheric link in a 1 m laboratory link.

Chapter 3

Phase sensitive parametric amplifiers

Phase sensitive amplifiers (PSAs) are known to achieve low noise amplification of optical signals, ideally adding no noise (NF = 0 dB) whereas the conventional EDFAs can have NF of 3 dB. EDFAs operate on electronic transitions between energy levels whereas PSAs operate by parametric amplification and coherent addition of optical signals due to a nonlinear phenomenon such as four-wave mixing or sum/difference frequency generation [36–40].

PSAs were first conceptualized in the year 1982 [41], where the author shows that there exists a bandwidth dependent lower limit on the noise added in one quadrature of signal. This was first experimentally demonstrated in χ^2 material [42] then using χ^3 material [43]. Later PSAs were considered for different possible configurations for a fiber such as single mode, two-mode and multi mode [44] and it has been realized in real fiber optic communication environment [24] used as inline amplifier. It has also been used as regenerator for fiber transmission links by squeezing the phase and amplitude noise [23]. Recent demonstrations show that PSAs can be used to reach 6 times higher transmission distance compared to EDFA [45]. In this thesis we show the prospects of using PSA as highly sensitive pre-amplifier for receivers in free-space communications due to the 3 dB noise figure benefit over EDFA. Two main mechanisms behind the operation of PSA are the four-wave mixing and parametric amplification process in a χ^3 nonlinear medium which are discussed in this chapter.
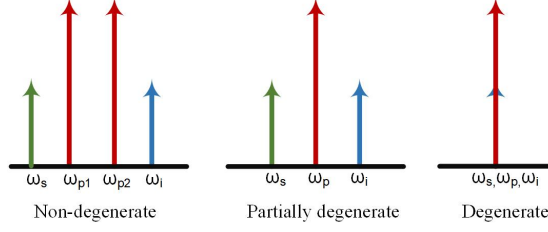
Figure 3.1: Four wave mixing schemes

3.1 Four-wave mixing

Four-wave mixing is a third order nonlinear phenomenon where three optical waves of different frequencies interact in a nonlinear χ^3 medium to generate the fourth frequency by satisfying the conservation of energy and momentum of photons incident [46]. If the three wave mixing frequencies are different, it is called non-degenerate four-wave mixing and if two of the mixing frequencies are identical, it corresponds to partially degenerate case and if all are same, it is called completely degenerate four-wave mixing [47]. The generated frequency is called idler, conjugate or satellite [46]. The name conjugate is used because four-wave mixing is mostly used in the partially degenerate case with a single pump and a signal interact to generate a conjugate of the signal. However the generated wave need not be a conjugate of signal in general. Fig. 3.1 show the classification of all the three configurations.

In this thesis, we study the partially degenerate case where a pump wave interact with a weaker signal to generate the idler wave. In order to satisfy the conservation of energy and momentum the frequency of pump related to signal and idler by $2\omega_p = \omega_s + \omega_i$ and propagation constant $2\beta_p = \beta_s + \beta_i$ where p, s, i are notations of the pump, signal and idler. The generated idler power is proportional to the square of injected pump P_p^2, signal power P_s and the phase mismatch factor. The expression for idler power is given by [48].

$$P_i(L) = 4\eta_i \gamma^2 P_p^2 P_s e^{-\alpha L} \left(\left| \frac{1 - e^{-\alpha L}}{\alpha} \right|^2 \right) \tag{3.1}$$

where α, γ are the attenuation coefficient, nonlinear coefficient of the HNLF and η is the FWM efficiency, which depends on the phase mismatch factor given by [49].

$$\eta = \left(\frac{\alpha^2}{\alpha^2 + \Delta\beta^2} \right) \left[1 + \frac{4e^{-\alpha L} \sin^2(\Delta\beta L)}{|e^{-\alpha L} - 1|^2} \right] \tag{3.2}$$

where $\Delta\beta = 2\beta_p - \beta_s - \beta_i$ is the phase mismatch, if $\Delta\beta = 0$, the FWM

efficiency becomes 1 i.e., maximum. Due to dispersion in the HNLF the pump, signal and idler waves travel at different velocities, resulting in finite phase mismatch $\Delta\beta$ and hence the conversion efficiency is less than 1.

3.2 Parametric amplification

When a high power pump is launched into a HNLF, noise around the pump will start experiencing amplification as the energy of the pump gets transferred to higher and lower frequencies satisfying energy and momentum conservation. This can be described as FWM process under phase matching. If a weak signal wave is present instead of noise in the gain region, it will see an amplification and also generate a idler via FWM. The shape of the gain spectrum depends on the pump power and phase matching condition in the fiber. Parametric gain can be understood in more detail using the propagation equations of pump, signal and idler waves. These are obtained by substituting the fields of these waves in nonlinear Schrödinger equation and are given by [25],

(Note that the terms related to self-phase modulation and cross-phase modulation are ignored here)

$$\frac{dP_p}{dz} = -4\gamma(P_p^2 P_s P_i)^{1/2}\sin\theta \tag{3.3}$$

$$\frac{dP_s}{dz} = \frac{dP_i}{dz} = 2\gamma(P_p^2 P_s P_i)^{1/2}\sin\theta \tag{3.4}$$

and

$$\frac{d\theta}{dz} = \Delta\beta + \gamma(2P_p - P_s - P_i) + \left(\sqrt{\frac{P_p^2 P_s}{P_i}} + \sqrt{\frac{P_p^2 P_i}{P_s}} + 4\sqrt{P_s P_i}\right)\cos\theta \tag{3.5}$$

where $\theta = \phi_p - \phi_s - \phi_i$.

ϕ_p, ϕ_s and ϕ_i are the absolute phases of pump, signal and the idler. In Eq. (3.3) and Eq. (3.4), the negative and positive sign on the right hand side indicate the pump power is attenuated and the signal and idler being amplified as they propagate in the fiber. This transfer of energy depends on the relative phase value θ and should ideally $\pi/2$ to have maximum energy transfer from pump to signal and idler.

If $\theta = \pi/2$ in the Eq. (3.5), the last term will be zero and to stay phase matched we need

$$\kappa = \Delta\beta + \gamma P_p = 0 \tag{3.6}$$

This assumes that the pump power is much higher than the signal and idler power.

It is clear from Eq. (3.6) that in order to have perfect phase matching, $\Delta\beta$ should be negative. If the pump frequency is close to the zero-dispersion frequency of the HNLF ω_0, then the phase matching condition can be written approximated as

$$\kappa = \beta_3(\omega_p - \omega_0)(\omega_s - \omega_p)^2 + \gamma P_p = 0 \tag{3.7}$$

Here β_3 is the third derivative of the propagation constant at ω_0. Eq. (3.7) shows that, to have the phase matching condition condition satisfied the difference $\omega_p - \omega_0$ must be negative. In other words, the pump frequency should be in the anomalous dispersion regime to have maximum parametric gain. Assuming no pump depletion and a weak signal, the analytical solutions for the signal gain is given by

$$G = \left(1 + \frac{\gamma P_p}{g}\sinh(gL_{eff})\right)^2 \tag{3.8}$$

where L_{eff} is the effective length of the fiber defined by $L_{eff} = [1 - e^{-(\alpha L)}]/\alpha$ and g is the parametric gain coefficient given by

$$g = \left[(\gamma P_p)^2 - \left(\frac{\kappa}{2}\right)^2\right] \tag{3.9}$$

Under perfect phase matching ($\kappa = 0$) the expression for the signal gain can be simplified to

$$G = \frac{1}{4}\exp(2\gamma P_p L_{eff})) \tag{3.10}$$

From the Eq. (3.10) we can infer that, the signal will grow exponentially with respect to the pump power if the phase matching condition is satisfied. This gain region is also called exponential gain regime due to the exponential dependence of gain on the pump power. The gain dependence on pump power can become quadratic if the signal wavelength is close to the pump. However, this condition is not relevant for discussion in this thesis as we operate in the exponential gain regime. The maximum amount of pump power is typically limited by the Brillouin scattering threshold, the power level above which pump will start reflecting back due to acoustic phonon vibrations in the HNLF.

3.3   Quantum noise

Quantum mechanics predicts that the quantum state with zero photons has finite energy, termed as vacuum energy state or zero point energy state. The value of zero point energy for a single mode with frequency ν is $h\nu/2$. As the name indicates, it originates from the zero point fluctuation of the electromagnetic field. This results in measurement uncertainty of coherent state.

let $\hat{a}_1$ and $\hat{a}_2$ are the inphase and quadrature phase complex fields and $\langle \Delta \hat{a}_1 \rangle$, $\langle \Delta \hat{a}_2 \rangle$ are the uncertainties associated with I and Q quadratures. According to Yamamoto in [50], coherent state is one of the minimum uncertainity state satisfies the following relations, also satisfied by Heisenberg's uncertainity relations

$$\left\langle \Delta \hat{a}_1^2 \right\rangle \left\langle \Delta \hat{a}_2^2 \right\rangle = \frac{1}{16} \qquad (3.11)$$

for each quadrature [50],

$$\left\langle \Delta \hat{a}_1^2 \right\rangle = \left\langle \Delta \hat{a}_2^2 \right\rangle = \frac{1}{4} \qquad (3.12)$$

where $\left\langle \Delta \hat{a}_i^2 \right\rangle_{i=1,2}$ denote the variance of the uncertainty of each quadratures. The inphase and quadrature phase of the coherent state are equally noisy and have minimum uncertainties given by Eq. (3.12). These flutuations $1/4$ of photon energy for each of the quadrature [50].

Simultaneous IQ measurement

For coherent state of light, simultaneous measurement is the measurement of in-phase component doesn't effect the succeeding measurement of quadrature phase component and vice versa.

The quantum mechanical uncertainty associated with simultaneous I and Q measurement exceeds the uncertainty associated with coherent state of light discussed before. The uncertainty product of measurement is 3 dB larger than the one dictated by the uncertainty principle. This is due to simultaneous measurement requires internal mode fluctuations to allow for commutation of the two simultaneously measured operators. These fluctuations increase the uncertainty by 3 dB from the uncertainty product of input operators. [50].

However, single observable measurement (one quadrature) is free of excess noise and therefore uncertainty product of two independent single observables (independent quadratures) is reduced to uncertainty relation discussed Eq. (3.13) [50]. Hence, the measurement uncertainty of coherent state of light is given by [50, 51]

$$\left\langle \Delta \hat{x}_1^2 \right\rangle \left\langle \Delta \hat{x}_2^2 \right\rangle \geqslant \frac{1}{4} \qquad (3.13)$$

where $\left\langle \Delta \hat{x}_1^2 \right\rangle$ and $\left\langle \Delta \hat{x}_2^2 \right\rangle$ are the measurement uncertainties associated with I and Q quadratures.

It can be seen that, once we make measurement with least uncertainty in one quadrature of coherent state, which is $\left\langle \Delta \hat{x}_1^2 \right\rangle = 1/4$, we add infinite uncertainty in the other quadrature.

A single quadrature measurement can be performed with minimum noise energy $h\nu/4$, and Simultaneous measurement of I and Q require twice the
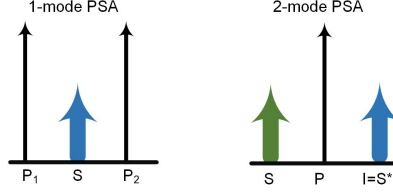
Figure 3.2: Different PSA schemes

uncertainty dictated by the measurement uncertainty principle, which is $h\nu/2$ in each quadrature or $h\nu$ in both quadratures.

This uncertainty in measurement is also applicable to optical amplifiers where the amplification process results in additional noise, discussed in next section.

3.3.1 Amplifier noise

EDFAs amplify a signal by population inversion which is associated with spontaneous emission noise because of the gain medium, whose power spectral density is given by the expression

$$S_{sp}(\nu) = (G-1)n_{sp}h\nu \tag{3.14}$$

where ν is the optical frequency and n_{sp} is the spontaneous emission factor or population inversion factor given by $N_2/(N_2 - N_1)$. where N_1 and N_2 are the atomic populations of the ground and excited states respectively.

The noise figure of the, which is the ratio of input SNR to output SNR is given by

$$F = 2n_{sp}(G-1)/G \approx 2n_{sp} \tag{3.15}$$

The minimum value of n_{sp} is 1, resulting in a minimum 3 dB noise figure, which means the amplifier adds excess noise to the input quantum noise limited signal. A PSA amplifies one quadrature without adding any additional noise and squeezing the noise in other quadrature while attenuating it. This results in single quadrature measurement with least uncertainty $h\nu/4$.

A two mode PSA amplifies both quadratures of light simultaneously where we need two input waves at different frequencies. Figure shows one-mode, two-mode phase sensitive amplification schemes which amplify single and both quadratures of light simultaneously.

In the first case, i.e., the one-mode PSA, the signal and idler are degenerate and is in between the two CW pumps in frequency domain. The signal and one of the pumps originate from two separate free-running lasers, the second

pump must be locked with the phase $\theta_{p2} = 2\theta_s - \theta_{p1}$. By coherent addition signal and the generated idler at the same frequency, one of the quadratures of the signal gets amplified and other quadrature gets attenuated.

In the second case, the two-mode PSA, a non-degenerate signal and idler pair at different frequencies and a cw-pump in the configuration shown in Fig. 2. The pump must be phase locked to the signal and idler and satisfy the relation $\theta_i = 2\theta_p - \theta_s$. By coherent addition of signal and conjugated idler, both the quadratures of the signal will experience amplification. The detailed derivation of the amplification will presented in the next section.

A two-mode PSA can amplify both quadratures of signal simultaneously noise-free, by using two input waves. This can understood as two one-mode amplifiers, amplifying each of the two quadratures of coherent light.

3.4 Phase sensitive amplification - Transfer matrix approach

Eq. (3.8) and Eq. (3.9) describe the gain of parametric amplifier with a single input wave. If for the phase sensitive case, where a non zero idler also present at the input, we need a more sophisticated model to understand the process. A transfer matrix describing the fields of signal and idler at output of parametric amplifier in terms of input fields is given as

$$\begin{bmatrix} B_s \\ B_i \end{bmatrix} = \begin{bmatrix} \mu & \nu \\ \nu^* & \mu^* \end{bmatrix} \begin{bmatrix} A_s \\ A_i^* \end{bmatrix} \tag{3.16}$$

The matrices A and B correspond to the input and output of the parametric amplifier. s and i denote signal and idler waves, * denotes the complex conjugate. μ and ν are complex transfer coefficients given by.

$$\mu = \cosh(gL) - i\frac{\kappa}{2g}\sinh(gL) \tag{3.17}$$

$$\nu = i\frac{\gamma P_p}{2g}\sinh(gL) \tag{3.18}$$

It is important that μ and ν satisfy the relation [52]

$$|\mu|^2 - |\nu|^2 = 1 \tag{3.19}$$

From Eq. (3.16) the output signal is obtained by coherent addition of input signal and conjugated idler multiplied by their coefficients μ and ν. Rewriting the interacting fields in terms of powers by considering $A = \sqrt{P}e^{j\phi}$, the signal gain is obtained as

$$G_{PSA,s} = \frac{|B_s|^2}{|A_s|^2} = |\mu|^2 + \frac{|\nu|^2 P_{i0}}{P_{s0}} + 2|\mu||\nu|\sqrt{\frac{P_{i0}}{P_{s0}}}\cos(\phi_\mu + \phi_\nu + \theta_{rel}) \tag{3.20}$$

19

Here P_{i0}, P_{s0} are input idler and signal powers. $\phi_{\mu,\nu}$ denote the phase angles of the complex transfer coefficient and we have introduced the relative phase $\theta_{rel} = \phi_s + \phi_i$, is the phase angle measured relative to the pump. For zero input idler power, the gain is simply $|\mu^2|$ and is the phase in-sensitive parametric gain denoted by G earlier in Eq.(3.8)

The maximum achievable PSA gain in Eq.(3.20) is

$$G_{PSA,s} = \frac{(\sqrt{GP_{s0}} + \sqrt{(G-1)P_{i0}})^2}{P_{s0}} \tag{3.21}$$

$$G_{PSA,i} = \frac{(\sqrt{GP_{i0}} + \sqrt{(G-1)P_{s0}})^2}{P_{i0}} \tag{3.22}$$

It can also be shown that, the PSA minimum gain is $1/G_{max}$ which means PSA can attenuate by the same factor as it can amplify. When input signal and idler have identical power, phase sensitive gain will be 4 times the in-sensitive gain $G_{PSA,s} = 4G$

3.4.1 Noise figure

Until now we have assumed signal without any noise. In reality, PSA is limited by quantum noise, which is also considered as zero point energy or vacuum energy given by $h\nu/2$ at a given frequency ν. Quantum noise can be statistically expressed similar to additive Gaussian noise. Quantum noise is considered to be uncorrelated at all frequencies, thus $\langle n_s n_i \rangle = 0$, $\langle n_s \rangle = 0$ and $\langle |n_s|^2 \rangle = h\nu/2$. where $\langle . \rangle$ is the expectation operator and n_s, n_i are noises at signal and idler. The transfer matrix model is now written as

$$\begin{bmatrix} B_s \\ B_i \end{bmatrix} = \begin{bmatrix} \mu & \nu \\ \nu^* & \mu^* \end{bmatrix} \begin{bmatrix} A_s + n_s \\ A_i^* + n_i^* \end{bmatrix} \tag{3.23}$$

Since n_s and n_i are uncorrelated, the amplification of noise will be $|\mu|^2 + |\nu|^2$. We know that the gain of a PIA is $G = |\mu|^2$, we can thus write the noise gain $G_{noise} = |\mu|^2 + |\nu|^2 = 2G - 1$. The noise figure can be written as

$$NF = (SNR_{in})/(SNR_{out}) = G_{noise}/G_{sig} \tag{3.24}$$

substituting the expressions for signal gain and noise gain in the Eq. (3.24), for phase in-sensitive amplifier

$$NF_{PIA} = \frac{2G - 1}{G} \tag{3.25}$$

and for the phase sensitive amplifier

$$NF_{PSA_s} = \frac{(2G-1)P_{s0}}{(\sqrt{GP_{s0}} + \sqrt{(G-1)P_{i0}})^2} \tag{3.26}$$

$$NF_{PSA_i} = \frac{(2G-1)P_{i0}}{(\sqrt{GP_{i0}} + \sqrt{(G-1)P_{s0}})^2} \tag{3.27}$$

In the approximation $G >> 1$ and $P_{so} = P_{io}$ which is practical case, $NF_{PIA} = 2$ (3 dB) and $NF_{PSA} = 1/2$ (-3 dB). Since PSA has both signal and idler as inputs, we need to account for idler power also. The combined noise figure for PSA will be

$$NF_c = NF_s + NF_i = NF_s \frac{P_{s0} + P_{i0}}{P_{so}} \tag{3.28}$$

This means that the combined noise figure is approximately equal to summation of signal and idler noise figures. If $P_s = P_i$ then the $NF_c = 1$ or 0 dB.

Chapter 4

High sensitivity optical communications

4.1 Optical receiver sensitivity

In chapter 2, we discussed different ways of improving the received power in a long haul free-space link. The communication performance is dictated by receiver sensitivity measured in photons per bit for error free detection. The Receiver sensitivity depends on three factors. 1. The receiver's ability to detect received photons with minimum noise possible 2. Modulation format 3. Forward error correction codes. This chapter deals with the aspects of modulation and reception of light to achieve lowest receiver sensitivity by different methods and their drawbacks.

4.1.1 Coherent receivers

Two types of receivers can be used in space communication, coherent receivers and direct detection receivers. The statistical nature of channel output depends on the detection method, which is Gaussian in the case of coherent and Poissonian for direct detection for very low received powers. In coherent receivers, the received signal is beat with a strong local oscillator (LO) and the beat signal is detected in one or both quadratures using photo detectors as shown in Fig 4.1. The local oscillator power is usually more than 10 mW and the received signal power in the range of micro watt or lower. Due to the beating of the strong LO with a weak signal, the noise level of signal increases much above the detector thermal noise. A coherent receiver is thus limited by shot noise due to the power of local oscillator. Low quantum efficiency of the detectors can limit the signal to noise ratio (SNR) of received signal and hence pre-amplifier is used to amplify the signal before detection, where its noise figure will be limiting the
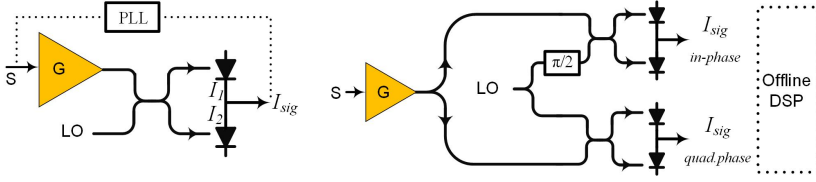
Figure 4.1: Pre-amplified single (left) and dual quadrature(right)coherent receiver

performance.

A typical pre-amplified coherent receiver for measuring single and both quadratures of light are shown in the Fig 4.1.

The derivation of signal's SNR after coherent receiver has been shown in the literature multiple times, but different authors claim different results. For example Kikuchi in [53] claims the shot noise limited SNR for a phase diversity receiver (dual quadrature receiver) to be n_s where n_s is the average number of photons-per-symbol. Whereas the same author claims SNR of $2n_s$ in his paper in 2015 [51] contradicting the previous result. The paper on coherent detection by Ezra Ip in [54] claims that the SNR of phase diversity receiver is $2n_s$ which is same as single quadrature receiver, this result agrees with Agrawal.G.P [55] in dual quadrature receiver but not with single quadrature case. Leong in his paper in [56] claims that SNR of single quadrature and dual quarature receiver is $2n_s$ and provides a complete list of references who agrees and disagrees with their result.

Out of these different results, it is very important to have a correct one as this is required for theoretical analysis of the PSA based receiver. Hence, we provide a derivation of the SNR of single and dual quadrature receivers under shot noise limit and also pre-amplified coherent receivers under amplified spontaneous limit (ASE) noise limit. Our result agrees with our experimental result including experimental penalties. An intuitive explanation was given in paper D supplementary.

Fig. 4.1 shows the schematic of single and dual quadrature pre-amplified receivers for receiving single polarisation coherent signal. An external electrical phase locked loop is used in the single quadrature receiver to track the phase of the signal with respect to local oscillator (LO). Whereas in dual quadrature receiver, offline digital signal processing techniques can be used to recover the laser phase as both quadratures of signal are detected, which is not possible with single quadrature detection.

Single quadrature receiver

For a single quadrature pre-amplified receiver, the photo current at the output of each of the photodiodes is given by

$$I_1(t) = R\left[\frac{GP_S}{2} + \frac{P_{LO}}{2} + 2\sqrt{\frac{GP_SP_{LO}}{4}}cos(\omega_{IF}t + \phi_S - \phi_{LO})\right] \qquad (4.1)$$

$$I_2(t) = R\left[\frac{GP_S}{2} + \frac{P_{LO}}{2} - 2\sqrt{\frac{GP_SP_{LO}}{4}}cos(\omega_{IF}t + \phi_S - \phi_{LO})\right] \qquad (4.2)$$

where P_S is the signal power, P_{LO} is the LO power, ω_{IF} is difference in frequency between signal and LO, ϕ_S and ϕ_{LO} are the phases of signal and LO. G is the pre-amplifier gain, R is the responsivity of the photodetector, which is related to the quantum efficiency η by the relation, $R = \eta q/h\nu$, where q, ν and h are the electron charge, photon frequency and planks constant.

The combined photo current is the difference of individual photo currents generated, given by

$$I_{sig} = I_1 - I_2 = R[2\sqrt{GP_SP_{LO}}cos(\omega_{IF}t + \phi_S - \phi_{LO})] \qquad (4.3)$$

where the DC terms will be eliminated due to subtraction of the currents and the resulting beat-term doubles. This detection is also called balanced detection.

The electrical signal power is

$$\overline{I_{sig}^2} = [2R\sqrt{GP_SP_{LO}}cos(\omega_{IF}t + \phi_S - \phi_{LO})]^2 \qquad (4.4)$$

In homodyne receiver, the term $cos(\omega_{IF}t + \phi_S - \phi_{LO}) = 1$ as frequency and phase of the signal and LO are same, the signal power is

$$\overline{I_{sig}^2} = 4R^2GP_SP_{LO} \qquad (4.5)$$

Noise sources for a pre-amplified coherent receiver are mainly the ASE of the pre-amplifier and shot noise due to the LO.

The ASE power over the signal bandwidth B , in one polarisation mode is given by

$$P_{ASE} = S_{ASE}\Delta f = n_{sp}(G-1)h\nu B \qquad (4.6)$$

where n_{sp} is the spontaneous emission factor,S_{ASE} is the power spectral density in one polarisation, G is the gain of the pre-amplifier. The electric filed of ASE over a arbitrary small frequency width $\delta\nu$, centered at frequency ω_{ASE} is

$$E_{ASE} = \sqrt{n_{sp}(G-1)h\nu\delta\nu}cos(\omega_{ASE}t + \phi_{ASE}) \qquad (4.7)$$

where ϕ_{ASE} is random phase of each component of spontaneous emission. The corresponding ASE power over a small frequency width $\delta\nu$ is $N_{ASE} = | E_{ASE} |^2$

The noise power is the electrical beat of ASE noise and LO over a small frequency width $\delta\nu$ given by (ignoring the DC terms due to balanced detection)

$$\overline{I^2_{ASE}} = [2R\sqrt{P_{LO}N_{ASE}}cos((\omega_s - \omega_{ASE})t + \phi_S - \phi_{ASE})]^2 \qquad (4.8)$$

The beat of ASE and LO should be treated like a heterodyne beating due to the random phase difference, hence the beat term $cos((\omega_s t - \omega_{ASE}t) + \phi_S - \phi_{ASE}) = 1/\sqrt{2}$,

Note that, the signal power is much lower than LO and hence signal-ASE beat is neglected in equation.

This results ,

$$\overline{I^2_{ASE}} = 2R^2 G P_{LO} N_{ASE} \qquad (4.9)$$

In case of dual polarisation signal, the noise term doubles. However, we discuss only single polarisation signal in this thesis.

The electrical noise power due to ASE in the receiver bandwidth Δf is

$$\overline{\sigma^2_{ASE}} = \overline{I^2_{ASE}}\Delta f = 2R^2 G P_{LO} n_{sp}(G-1)h\nu\Delta f \qquad (4.10)$$

Note that the receiver bandwidth Δf can be approximated as $\Delta f = B/2$. As S_{ASE} is two sided power spectral density of ASE in optical domain, after homodyne detection, only one sided PSD is considered, i.e., noise from both sides folds into one side, resulting twice the ASE power. Hence Eq. (4.10) becomes

$$\overline{\sigma^2_{ASE}} = 4R^2 G P_{LO} n_{sp}(G-1)h\nu\Delta f \qquad (4.11)$$

Hence the SNR of single quadrature homodyne receiver is

$$SNR = \frac{\overline{I^2_{sig}}}{\overline{\sigma^2_{shot}} + \overline{\sigma^2_{ASE}}} = \frac{4R^2 G P_S P_{LO}}{2Rq P_{LO}\Delta f + 4R^2 G P_{LO} n_{sp}(G-1)h\nu\Delta f} \qquad (4.12)$$

where the shot noise due to LO power is

$$\overline{\sigma^2_{shot}} = 2Rq P_{LO}\Delta f \qquad (4.13)$$

As discussed before, the shot noise due to LO could also be dominating when the ASE power is low, caused by lower amplifier gain.

The Eq. (4.12) can be simplified to

$$SNR = \frac{P_S}{\frac{q\Delta f}{2RG} + n_{sp}(G-1)h\nu\Delta f} \qquad (4.14)$$

By substituting the expressions for responsivity $R = \eta q/h\nu$, signal power $P_S = h\nu B n_s$ where n_s is the number of photons per symbol and receiver bandwidth $\Delta f = B/2$, and simplifying further,

$$SNR = \frac{4Gn_s}{\frac{1}{\eta} + 2Gn_{sp}} \tag{4.15}$$

Assuming the gain of pre-amplifier is large, ASE noise term dominates over the shot noise, then the SNR is simplified to

$$SNR = \frac{2n_s}{n_{sp}} \tag{4.16}$$

The spontaneous emission factor n_{sp} related to the noise figure of the amplifier by $F = 2n_{sp}$ for EDFA. We can simply re-write the SNR equation to $SNR = 4n_s/F$

For a shot noise limited system, i.e., when pre-amplifier was not used, ignoring the second term in the denominator and assuming $G = 1$, the received SNR is given by

$$SNR_{shot} = 4\eta n_s \tag{4.17}$$

We see that SNR of the shot noise limited system depends on quantum efficiency of the photo detector. Typical commercial coherent receivers have very low quantum efficiency 10 % approximately.

From Eq. (4.15), it is clear that the gain of the pre-amplifier G should be sufficiently high to overcome the quantum efficiency of the photo-detector η to see a clear advantage of using pre-amplifier. However, the minimum noise figure of any pre-amplifier is 3 dB, Pre-amplifier reduces the SNR by a factor of 2 compared to ideal shot noise limited SNR given in Eq. (4.17), considering the pre-amplifier is EDFA with $n_{sp} = 1$. If one were to consider a phase sensitive pre-amplifier (either one-mode or two mode configuration) to amplify the signal instead of EDFA, one can achieve the ideal shot noise limited SNR.

A similar analysis can be carried out for dual quadrature (DQ) coherent receiver shown in Fig 4.1, where two single quadrature coherent receivers used for both I and Q quadratures, where the signal, local oscillator and ASE were split into half for each quadrature.

Dual quadrature receiver

To calculate the SNR of a DQ pre-amplified receiver, we need to replace $P_S \rightarrow P_S/2$, $P_{LO} \rightarrow P_{LO}/2$ and $P_{ASE} \rightarrow P_{ASE}/2$ for each quadrature in the Eq. (4.12).

$$SNR = \frac{4R^2 G \frac{P_S}{2} \frac{P_{LO}}{2}}{2Rq\frac{P_{LO}}{2}\Delta f + 4R^2 G\frac{P_{LO}}{2}\frac{n_{sp}(G-1)h\nu\Delta f}{2}} \tag{4.18}$$

$$= \frac{P_S}{n_{sp}h\nu\Delta f} = \frac{2P_S}{n_{sp}h\nu B} = \frac{2n_s}{n_{sp}}$$

The SNR remains same as that of SQ pre-amplifier if the ASE-LO beat noise dominates over the shot noise. However, in the shot noise limited case the SNR degrades by a factor of 2 due to the reduction of the signal power whereas the the local oscillator power cancels out in numerator and denominator, having no influence on the result.

The SNR of DQ pre-amplified receiver in shot noise limited case is

$$SNR_{shot} = \frac{4R^2G\frac{P_S}{2}\frac{P_{LO}}{2}}{2Rq\frac{P_{LO}}{2}\Delta f} = 2\eta n_s \tag{4.19}$$

which is half of the SNR of SQ receiver. For the EDFA pre-amplifier case, the SNR both SQ and DQ receiver remains same and equal to ideal shot noise limited DQ receiver SNR $SNR = 2n_s$.

By using a PSA pre-amplifier instead of EDFA, the SNR is 3 dB higher than EDFA and it equals the single quadrature shot noise limited SNR $4n_s$. PSA's used to amplify one quadrature of the signal, called one-mode PSA [22]. Two-mode PSAs are used to amplify both quadratures [44], yet providing the same 0 dB noise figure. The implementation of two-mode PSA will be discussed in the next chapter.

It is important to note that, detecting both the quadratures allows using higher order modulation format, which is not possible in single quadrature case.

4.1.2 Direct detection

In a direct detection receiver, the optical intensity is detected and there is no need of further processing as in coherent detection. Direct detection is usually limited by thermal noise, given by $\sigma_T^2 = (4K_BT/R_L)F\Delta f$. where T is the ambient temperature and K_B is Boltzman's constant, R_L is the load resistance of the detector circuit and Δf is the bandwidth.

Photon counting direct detection receivers are mostly used as direct detection receivers in free-space communication and are in practice cooled down to few Kelvin to reduce the effect of thermal noise [7]. According to [57], photon counting receivers can achieve higher sensitivity than coherent detection by choosing an appropriate modulation format such as M-ary pulse position modulation (M-PPM), provided photon counting detectors operate under low thermal noise conditions.

By assuming thermal-noise-free direct detection, the received SNR will be dictated by the arrival statistics of the photons following Poissonian distribution.

Suppose n_s is the mean number of photons arrived at the receiver, the probability of receiving k photons at that interval by Poissonian statistics is
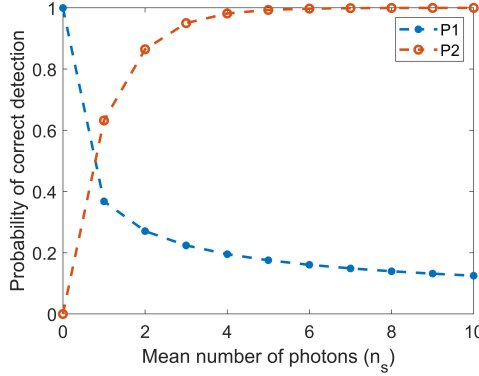
Figure 4.2: Probability of ON-OFF detection and multi-level detection ; $P1 = e^{-n_s} n_s^{n_s}/n_s!$ and $P2 = 1 - e^{n_s}$

given by

$$P(k) = \frac{e^{-n_s} n_s^k}{k!} \tag{4.20}$$

The mean and variance of the photon arrival statistics are same $SNR = n_s$. Note that, the Poissonian statistics are independent of size of the time interval or duration of observation and position of the interval of observation.

For ON-OFF keyed signals, the probability of detecting more than 0 photons is considered to be correct detection of the pulse. Hence the probability of detecting a pulse is $1 - P(0) = 1 - e^{n_s}$, which is greater than probability of detecting the exact number of photons as mean number, which is $P(n_s) = e^{-n_s} n_s^{n_s}/n_s!$ as shown in Fig. 4.2. Exact photon detection is required in a multilevel signal detection at low mean photon numbers.

The plot in Fig. 4.2 shows the probability of correctly detecting a pulse for ON-OFF signal scenario and multilevel signal scenario denoted by P_1 and P_2. The On-OFF signal probability is higher above mean of 1 photon. ON-OFF signals perform better than any other multilevel formats with direct detection. The SNR of direct detection receiver can be considered to be $SNR < n_s$ for a simple ON-OFF signal, for multilevel signal, $SNR = n_s$.

In deep-space communication, PPM format is widely used where ON-OFF signal is generated with ON pulse generated with low probability. Correctly detecting ON pulse can result in error free communication. In a typical deep-space link , background noise due to other radiations influence the received photon statistics. Ideal detection is not usually possible and the performance is much worse than ideal detection discussed here. [1]
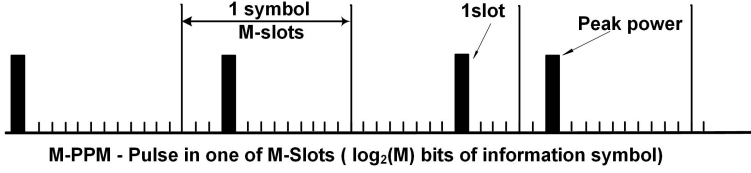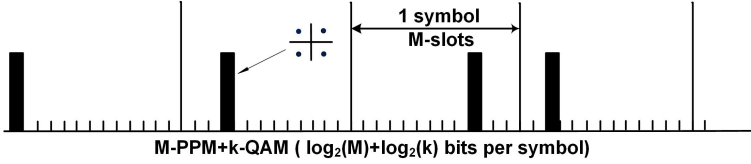
Figure 4.3: Example of M-ary PPM

Figure 4.4: Example of hybrid PPM+QAM modulation format

4.1.3 Modulation formats

PPM format with direct detection is the most widely used modulation scheme for free-space/deep-space communications due to its theoretical capacity to reach Shannon's limit at sufficiently large peak to average ratio [1]. In a M-ary PPM modulation scheme each temporal symbol is divided into M time slots and the information is conveyed by the time window by which the signal pulse is present. An illustration of M-PPM is shown in the Fig. 4.3

From the Fig. (3.2), to transmit $log_2(M)$ bits of information we need M time slots, but the power need to be only in 1 slot. Since the information lies in the position, the power efficiency can be improved by increasing number of slots (order of PPM) but this results in sacrificing spectral efficiency. The spectral efficiency of M-PPM format is $(\log_2 M)/M$ bits/s/Hz.

In space communications, a combination of pulse position modulation and direct detection using photon counting receivers is most widely used. In 2013 space mission to moon communicating by using lasers uses 16-PPM modulation format and nano-wire based photon counting receivers at earth operating at maximum downlink rate of 622 Mbps with slot rate of 5 Gslots per second.

Although PPM is a power efficient modulation format, its spectral efficiency is low, and this is important in the practical case of limited detection bandwidth. The maximum detection bandwidth of photon counting receivers is limited to few GHz. If one were to use 16-PPM or 32-PPM with such receivers, the maximum achievable information rate is limited to few 100s of Mbps considering FEC overheads. For future demands of high data rates in space communications, a transition from traditional PPM formats with direct detection to advanced QAM formats with coherent detection which are more
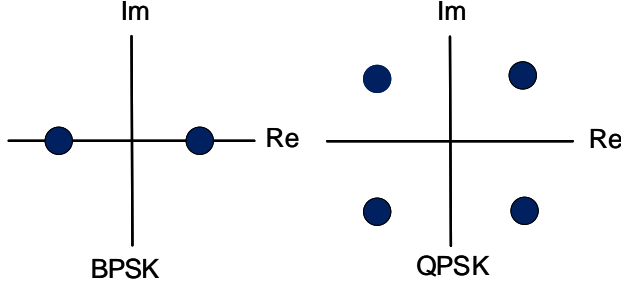
Figure 4.5: Constellation diagram of BPSK and QPSK

spectrally efficient, may be needed.

Simple QAM formats such as Binary phase shift keying (BPSK) and Quadrature shift keying (QPSK), where coherent detection can be used. Previous demonstrations of record sensitivities using coherent detection are [15, 58], where they show a sensitivities of error-free 2 PPB.
BPSK and QPSK constellations are shown in Fig. 4.5 where the phase of the optical field is modulated either in one or both quadratures, resulting in $\log_2 K$ bits/s/Hz, where K is the number of constellation points. The probability of bit error of rectangular K-QAM is given by [59]

$$BER_{K-QAM} = \frac{4(\sqrt{K}-1)}{\sqrt{K}\log_2 K}Q\left(\sqrt{\frac{3\gamma_b\log_2 K}{(K-1)}}\right) \tag{4.21}$$

where γ_b is the SNR per bit and K is the order of the QAM.

The probability of error of 4-QAM (QPSK) is $BER_{QPSK} = Q(2\gamma_b)$ which is the same as bit error probability of BPSK signal as a QPSK can be treated as two independent BPSKs [59].

Hybrid modulation, combining PPM with QAM can provide both higher spectral efficiency while improving sensitivity. In a M-PPM+K-QAM format, in each PPM's ON slot, QAM symbol is encoded as shown in Fig. 4.4 while m and k are the orders of PPM and QAM, This results in $\log_2 Km$ bits, with a spectral efficiency of $(\log_2 KM)/m$. There has been demonstration is the past on these formats achieving high sensitivity compared to pure-PPM and pure-QAM formats . [60, 61]

4.1.4   Channel coding

To perform error free communication over long distances, there are constraints on the modulation formats due to their implementation using physical devices. For example PPM enforces constraints on the relative location of pulses and describes the mapping of bits to the sequence of pulses.

On the other hand forward error correction (FEC) codes with soft decision decoding can be used to approach the Shannon's capacity limit. FEC adds redundancy to the transmitted information using a pre-determined algorithm. The redundant bits are complex functions of original information bits. This technique enhances the data reliability and error free communication. Typical FEC codes used for free-space communication are turbo codes and low density parity check LDPC codes. [1] The rate of a FEC code is $R = k/n$ where k is information word length in bits and n is codeword length, which is sum of information word length and redundant bits length. It can also expressed as overhead ratio, which is the ratio of redundant bits to information bits. For a rate-1/2 code, overhead ratio is 100 percent.

In Paper D we use a standard code used in telecommunications for satellite communications, which is a combination of 1/2 rate LDPC codes (100 % overhead) and very high rate BCH codes (low redundancy). This combination is used to have error free communication at all error rates.

4.2   Information capacity of different receivers

Shannon's information theory tells us the maximum rate at which information can be transmitted over a communication channel of a specified bandwidth in the presence of additive white Gaussian noise(AWGN) for error free communication [62], given by

$$C = B\log_2\left(1 + \frac{S}{N}\right) \tag{4.22}$$

where C is the channel capacity in bits per second, a maximum bit rate, B is the bandwidth of the channel in Hertz, S is the average received signal power, N is the average noise power within the bandwidth.

4.2.1   Capacity of coherent receivers

The above equation can be applied to all the coherent receivers discussed above. Complete derivations of capacities of all the receivers including shot noise limited, pre-amplified coherent receivers are presented in the Paper D supplementary section.

The general Shannon capacity of a homodyne receiver which uses k- dimensions (eg. quadratures, polarisations) for measuring information with a pre-amplifier having noise figure F given by

$$C_{coherent} = k \left(\frac{1}{2} B \log_2 \left(1 + \frac{4n_s}{kF} \right) \right) \tag{4.23}$$

For shot noise limited receivers, the noise figure F can be replaced with $1/\eta$ where η is the quantum efficiency of the detector. The value of k is 1 for single quadrature detection and 2 for dual quadrature detection.

For example, the capacity of a single quadrature (SQ) homodyne receiver in the shot noise limited (SN) case is given by

$$C_{homodyne} = \frac{1}{2} B \log_2 (1 + 4\eta n_s) \tag{4.24}$$

where $4\eta n_s$ is the SNR of the signal. The factor $1/2$ in front of the capacity is due to single quadrature (SQ) detection of the signal, i.e., only half of the capacity of the wave is used as one could transmit information in both quadratures.

Two mode PSA is a special case (discussed in paper D, in supplementary) where two separate channels are used to transmit the same information, utilizing twice the bandwidth. This results in a factor of $1/2$ in front of the capacity in Eq. (4.23). This is similar to the capacity of shot noise limited single quadrature receiver.

The sensitivity of a receiver is calculated from the capacity using the relation

$$\text{Sensitivity} \zeta = \frac{\text{photons-per-symbol}}{\text{spectral efficiency in bits-per-symbol}} = \frac{n_s}{C/B}. \tag{4.25}$$

For a SQ receiver in the SN-limit case, the sensitivity is

$$\zeta_{SQ-SN} = \frac{n_s}{\frac{1}{2} \log_2 (1 + 4\eta n_s)} \tag{4.26}$$

For $n_s \to 0$, this approaches $1/2\eta$.

4.2.2   Capacity of direct detection with PPM

As direct detection (photon counting detectors) results in Poissonian statistics, the probability of receiving at least one photon results in correct detection, is given by $1 - P(0) = 1 - e^{-n_s}$. The spectral efficiency of M-PPM is $SE_{PPM} = log_2 M/M$, the capacity of PPM, detected using photon counting receivers is thus

$$C_{PPM} = (1 - e^{-n_s}) \frac{log_2 M}{M} \tag{4.27}$$

where n_s is the average number of photons-per-symbol. For example, for 64-PPM, $C_{PPM} = 0.09(1-e^{-n_s})$ The corresponding sensitivity is simply $\zeta_{PPM} = 1/\log_2 M$

The Fig. 4.6 shows the sensitivities of the receivers discussed above. The ultimate capacity of a photon channel is the so-called Gordon's capacity or Holevo limit is obtained by considering photons as discrete particles being detected ideally with exact number without any uncertainty due to Poisson statistics [63].
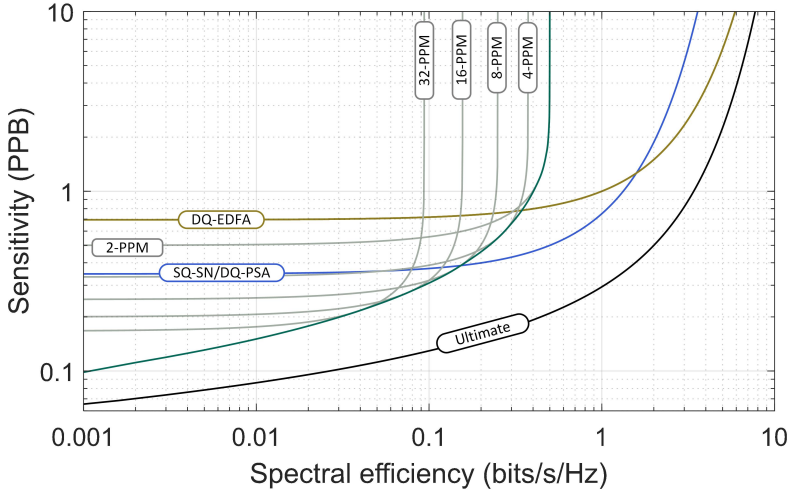
Figure 4.6: Spectral efficiency vs sensitivity of different receivers; DQ-EDFA, Dual quadrature coherent receiver with EDFA pre-amplifier; SQ-SN, Single quadratue shot noise limited receiver;DQ-PSA, Dual quadrature coherent receiver with PSA pre-amplifier; Ultimate: Ultimate capacity of a photon channel

$$C_{ultimate} = B\left(\log_2(1+n_s) + n_s\log_2\left(1+\frac{1}{n_s}\right)\right) \qquad (4.28)$$

Here n_s is the mean number of photons detected, the first term describes the classical information capacity of a channel and is predominant when average number of photons $n_s >> 1$ and the second term is of quantum origin, depends on photon arrival rate or probability of sending photons. Note that, in the limit of SNR $\rightarrow 0$, PPM approaches Gordon's capacity whereas coherent detection can achieve Gordon's capacity at very high SNR or spectral efficiencies.

Summary of capacities and sensitivities

All capacities of coherent homodyne receivers and their ultimate sensitivities are summarized in the Table. 4.1 and plotted in Fig. 2 with respect to spectral efficiency.

Receiver→	Single quadrature homodyne		Dual quadrature homodyne	
	Capacity	Best sensitivity	Capacity	Best sensitivity
SN limit	$B/2\log_2(1+4n_s)$	0.35 PPB	$B\log_2(1+n_s)$	0.7 PPB
EDFA pre-amp	$B/2\log_2(1+2n_s)$	0.7 PPB	$B\log_2(1+n_s)$	0.7 PPB
PSA pre-amp	$B/2\log_2(1+4n_s)$	0.35 PPB	$B/2\log_2(1+4n_s)$	0.35 PPB
	Direct detection			
M-PPM	$(1-e^{-n_s})\log_2 M/M$	$1/\log_2 M$ PPB		

Table 4.1: Summary of the capacities of all coherent receivers with their ultimate sensitivity limit

In the PSA capacity, the factor $1/2$ infront is due to two optical waves, the signal and idler carrying the same information. The SNR is 4times the SNR of EDFA receiver due to the fact that the noise figure of individual waves in PSA is $1/2$ or $-3dB$, where as the noisefigure of EDFA is 3dB, which is 4times higher than the NF of each waves.

At very low SNRs $\log(1+SNR) \approx SNR$, hence the capacity of PSA $(2Bn_s)$ is twice that of EDFA(Bn_s), and the corresponding sensitivity also doubles.

The immediate thought may be, can we improve the capacity by increasing number of modes of the PSA? It is not possible because the total noise figure of any mode PSA cannot be lower than 0 dB.

4.3 Capacity of N-mode phase sensitive amplifier
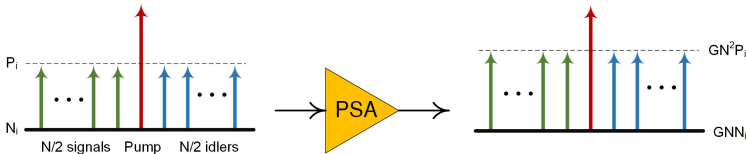

Figure 4.7: N-mode PSA configuration; G, Gain of the amplifier; P_i, input power of all the waves; N_i, input noise power; N, number of waves involved

Fig. 4.7 shows the N-mode configuration of the PSA, where N/2 signals and N/2 idler are involved in phase sensitive amplification process. As all the
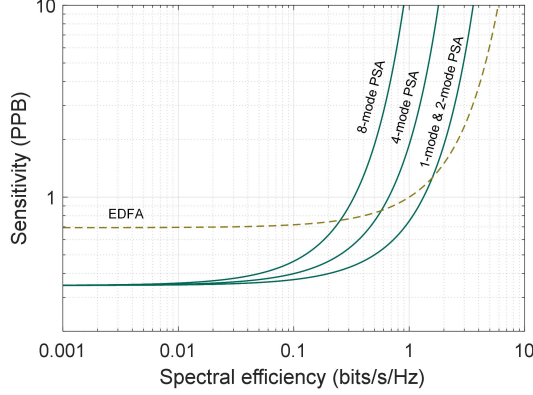
Figure 4.8: Sensitivity vs spectral efficiency of N-mode PSA compared

waves undergo coherent addition, the output power of each wave will be $N^2 G P_i$ where P_i is the power of input waves and G is gain of PSA, whereas due to incoherent addition of input quantum noise N_i, output noise power is NGN_i. This can be generalized to two-mode case, where only one signal and idler are present at the input. The noise figure of individual waves of N-mode PSA is $NF_{i=1:N} = 1/N$, for a two-mode PSA $NF_{i=1:2} = 1/2$ *or* 3 dB

The capacity of N-mode PSA is

$$C_{N-modePSA} = \frac{1}{N} B \log_2(1 + N \times 2n_s) \tag{4.29}$$

At low SNRs, the capacity remains the same as 2-mode PSA, while at high SNRs, $\log(1+\text{SNR}) \approx \log(\text{SNR}) \approx \log(2\text{SNR})$, and the capacity $C_{N-modePSA} = \frac{C_{2-modePSA}}{N}$ degrades by a factor of N compared to 2-mode PSA. Note that the capacity of 2-mode and 1-mode PSA are the same, the factor 1/2 in 1-mode PSA arises due to detecting singe quadrature of the wave.

We conclude that sensitivity can not be improved below the two mode PSA, however spectral efficiency keeps dropping as shown in Fig. 4.8

Block repeating and coherent combining

Block repeating and coherent combining is a technique to improve the SNR of the weak received signal and also used for data-rate scaling in space communications. This is accomplished by repeating the blocks of information sent multiple times and coherently or incoherently adding them in time domain.

In block repeating, each block of a specified number of data symbols, is repeated N times by the transmitter. The receiver then combines the repeated blocks in digital signal processing (DSP). The repeated block can be combined

incoherently by power combining for a $\sqrt{N}$ improvement in SNR, or coherently which results in an N improvement in SNR since the phases of the signals being combined can be phase aligned. Coherent combining is more efficient, but requires a phase sensitive receiver, such as a digital coherent receiver [15].

N-mode PSA accomplishes the same as that of block repeating. Instead of repeating time domain blocks,we can repeat in frequency domain by using N-frequency modes and performing PSA. In PSA, it is always guaranteed that waves are coherently added whereas in time domain block repeat, waves may not be coherently added and it depends on the phase noise of the signal.

Block repeating and coherent combining requires that the carrier phase be known and tracked for the total time duration of each set of block repeats to be coherently combined, whereas in N-mode PSA such tracking is not necessary.

One should also note that, time domain block repeating can complement the SNR gain of the N-mode PSA or in other words it can improve the received signal SNR and also allow improved data rate scaling.

4.4   Record sensitivity demonstrations

Free-space optical communications has been known since last few decades. Many attempts have been made to demonstrate a real deep-space optical communication link. The power requirements for deep-space links are typically high and hence it is challenging to establish link into deep-space. For communication to Moon requires at least 100 dB of power budget as the loss due to divergence itself is 80 dB and loss due to beam pointing and beam capturing can add further [64], considering a transmitter and receiver aperture sizes of about 10 cm, which is commonly used in space communications. Power efficiency or sensitivity has been an interesting topic of research in space communications over the years. Also there has growing interest in capturing more light using multiple apertures [14, 65].

Sensitivity is a measure of minimum number of photons required for error-free communication, in photons per bit. Table. 4.2 shows a list of record high sensitivity demonstrations in the past using various methods in free-space communication. Direct detection photon counting receivers along with PPM modulation formats were the interest in space community due to their low photon counting ability, but they suffer from low detection efficiencies at increased bandwidths. At high rates, optically pre-amplified receivers show best sensitivity, where amplifiers provide near ideal noise figures where as ideal shot noise limited systems suffer from quantum efficiency. Phase sensitive amplifier being the best known result at high rates, demonstrated in Paper D.

Table 4.2: List of high sensitivity optical receiver demonstrations; OH, Overhead ratio; SSPD, Photon counting NbN Super conducting single photon detector; SC-PPM, Serially concatenated pulse position modulation; LDPC, Low density parity check codes; PPM, Pulse position modulation; PS-QPSK, Polarisation switched quadrature phase shift keying; RS255/239, Reed-Solomon code 255/239

Rate (Gbps)	Sensitivity (avg. incident PPB)	Modulation	Receiver	Coding/OH	Ref.
10.5	1	QPSK	Intradyne	DVBS2,100 %	Paper D
0.014	1	32-PPM	Phot.cnt.SSPD	SC-PPM,100 %	[66]
0.038	1.45	16-PPM	Phot.cnt.SSPD	SC-PPM,100 %	[67]
0.156	1.5	BPSK	Homodyne	Turbo code,100 %	[68]
2.8	1.6	BPSK	Homodyne	LDPC, 300 %	[14]
5.69	1.73	QPSK	Intradyne	DVBS2, 300 %	[14]
11.65	2.04	QPSK	Intradyne	DVBS2,100 %	[14]
0.622	2.05	16-PPM	Phot.cnt.SSPD	SC-PPM,100 %	[67]
9.94	2.1	QPSK	Intradyne	DVBS2,100 %	[58]
0.128	2.3	64-PPM+PS-QPSK+4-FSK	Intradyne	no	[18]
6.23	2.7	4-PPM+PDM-QPSK	Intradyne	no	[61]
2.5	3.5	16-PPM+PDM-QPSK	Intradyne	no	[69]
20.69	3.71	QPSK	Intradyne	DVBS2, 10 %	[14]
19.88	3.9	BPSK	Homodyne	DVBS2, 100 %	[58]
0.073	4	256-PPM	Optical. Pre-amp	RS255/239, 7 %	[70]
40	4.3	PS-QPSK	Optical. Pre-amp	no	[71]
100	5.3	PDM-QPSK	Optical. Pre-amp	no	[71]
10	7	DPSK-RZ	Optical. Pre-amp	Turbo Block, 100%	[72]
10	7	DPSK-RZ	Optical. Pre-amp	Turbo Block, 100%	[72]

Chapter 5

Implementation of PSA for free space communication

A PSA is the lowest noise figure amplifier known, therefore ideally suited for free-space, but when used instead of EDFA, the transmitter should also be modified to achieve phase-sensitive operation. Fig. (5.1) shows the implementation of a PSA in a free space transmission link.

5.1 Free space link with PSA receiver

5.1.1 Transmitter

Unlike an EDFA, a PSA needs the signal, idler and, phase-coherent CW-pump waves as input to achieve a noise figure close to the 0 dB quantum limit. It is necessary that all the three waves are transmitted from the transmitter to the receiver. However, it is not mandatory to transmit the pump, and one could, in principle, generate the pump locally at receiver.

In our work, the signal was modulated with 10 GBaud QPSK data, where the data was encoded using forward error correction (FEC) code. The FEC code used here was second generation digital video broadcasting standard code (DVBS-2), which is used in modern satellite communications. The FEC encoded QPSK data was modulated on to the signal wavelength and combined with the CW pump to generate the conjugated wave called the idler.

Copier generation

In the copier stage, the data modulated signal and the pump wave are combined in an HNLF. Through the process of FWM, a conjugated copy of the signal called the idler wave was generated. A very narrow linewidth laser (100 Hz)
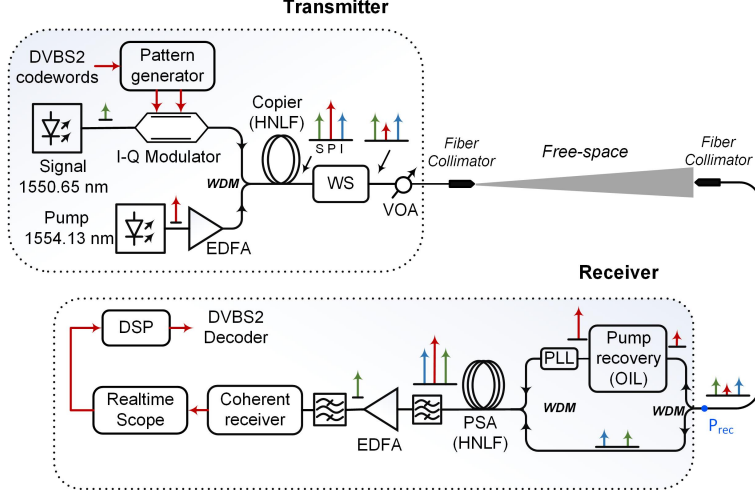
Figure 5.1: Setup for PSA implementation in a free space transmission link

was used as the pump, which makes the phase-locking of the pump, signal and idler waves in the PSA easier. The Copier is a 240 m long HNLF having a nonlinear coefficient of $11(Wkm)^{-1}$. The input signal and pump polarisation must be aligned for maximum conversion efficiency in the copier. The signal and pump wavelengths are chosen to maximise the signal gain according to the phase matching condition in the HNLF, which will be discussed later.

After the copier, the signal and idler were power balanced. The pump was attenuated to be 12 dB lower than the signal and the idler power using the wave-shaper so that the penalty from the transmitting pump is minimal. At the copier output, correlated quantum noise was generated at the signal and the idler wavelengths due to FWM. Since the signal and idler are attenuated by large amounts in the free space channel, the quantum noise becomes uncorrelated. Hence we can use the noise figure expressions are given by Eq. (3.26) in chapter 3.

5.1.2 Free space channel

As discussed in chapter 3, a 1 m long free-space link was used in the experiments to emulate the real deep space link, where the loss is due to divergence of the optical beam. We used fiber-coupled collimators at the transmitter and the receiver to couple light (all three waves signal, idler and the pump) into and from free-space. A variable optical attenuator was used to emulate the free-space loss after the transmitter. The collimators used at the transmitter and

40

the receiver had focal lengths of 0.38 mm and 2 mm. A collimator with larger focal length was used in the receiver to capture turbulence effects from the turbulence phase plate discussed in paper A. However for paper D, we did not use any turbulence plate.

The received power (for the sensitivity calculation) was measured after the receiver collimator. In free-space demonstrations, the sensitivity is measured along with the receiver optics' loss, similar to our demonstrations. Therefore, our results can be considered as a black-box sensitivity representing a realistic scenario.

5.1.3 Receiver

Pump penalty

In fiber communication systems with PSA as an inline amplifier, the pump wave is transmitted through the channel, but its power is not accounted into the receiver sensitivity as it does not occupy any significant bandwidth [73,74]. In free-space communication, it is necessary to include the pump power into the sensitivity calculation due to two reasons - the total received power must be accounted, and transmitter booster power will be distributed among three waves. If the pump was not transmitted, the booster power would be higher for signal and idler waves resulting in higher received signal power.

It is also possible to regenerate a phase-coherent pump at the receiver without transmitting through the channel. This requires a part of the received signal and idler waves [75]. Therefore, the pump should be transmitted along with the signal and idler to avoid sensitivity degradation.

The pump is separated from the signal and the idler waves by a WDM coupler with a low loss (0.1 dB) to avoid the sensitivity penalty at the receiver. The regenerated pump wave from injection locking is amplified using high power EDFA and combined with signal and idler in a HNLF stage for PSA with another WDM with a loss of 0.1 dB. The total loss due WDM couplers is 0.2 dB which causes the sensitivity penalty.

Phase sensitive parametric amplification

Nonlinear medium chosen for PSA was performed in a 4 stage HNLF with spools of lengths 103m, 128m, 164m and 204m spliced with isolators in between to reduce stimulated Brillouin scattering [26]. Each HNLF is strained with a linear strain across the length so as to increase the Brillouin threshold further [46] . All HNLFs were manufactured and strained by OFS Denmark. Straining the fiber increased the Brillouin threshold to be 500mW. After straining the fibers, the zero dispersion wavelength changes to 1543 nm from 1542 nm. The maximum pump power that can be injected into the PSA is 29 dBm, more than the Brillouin threshold resulting in maximum phase insensitive gain of 16

dB. As discussed in Chapter 3 the pump wavelength should be in anomalous dispersion region to have maximum exponential gain, we chose pump wavelength to be 1554.13 nm and the signal wavelength at 1550.65 nm in a region where maximum signal exponential gain can be achieved.

For maximum phase sensitive gain, the relative phase of all the waves at the input should be constant $\theta_{rel} = \phi_p - \phi_s - \phi_i = \pi/2$ as discussed in chapter 3. The paths of signal-idler and pump are different before reaching the PSA which the phase of the pump change randomly with respect to signal-idler. We employ a phase locked loop (PLL) to maintain the relative phase between signal, idler and pump. A small fraction of the amplified signal after the PSA is fed as input to the PLL, which then is sampled digitally in a micro-controller which generates an error signal proportional to the phase difference between the waves, which is used to vary the pump path using a PZT stretcher to achieve maximum phase sensitive signal gain.

The phase in-sensitive gain was 16 dB whereas phase sensitive gain was close to 22 dB. Due to the large free-space loss, the input signal power can be as low as -60 dBm resulting in an output signal to be only -38 dBm. The signal is amplified with an EDFA immediately after PSA with sufficient gain. It is important to not that the SNR of the signal will not degrade by introducing an EDFA after PSA as noise figure of PSA determines the noise figure of the combined amplifiers in a cascade system.

The signal is detected using a coherent receiver and data is captured using a real time scope. The data is post processed off-line with digital signal processing algorithms. The processing steps include In phase-Quadrature phase imbalance compensation, resampling of the received data to 2 samples per symbol. We further perform channel equalization by using constant-modulus algorithm for QPSK data resulting 1 sample per every symbol and then followed by frequency and phase estimation and compensation between the local oscillator and the signal waves [76].

DVBS2 code

DVBS2 code consists of a low-density parity check code (LDPC) with 100 percent overhead (1/2 rate) and BCH coded with a very high code rate. DVB-S2 operates over wide range code rates such as 1/4, 1/3, 1/2, 3/5, 2/3,3/4, 4/5, 5/6, 8/9 and 9/10 with four different modulation schemes, QPSK, 8-PSK, 16-APSK and 32-APSK. The QPSK modulation scheme performed the best among all at very low SNRs and therefore was used in our work. This is discussed in detail in paper E. We chose the 1/2 rate code as this was within 0.7 dB of Shannon's limit, close to rate-2/3 and 2/5 codes. Lowering code rate results in low SNR error-free communication but rates cause loss of spectral efficiency resulting in similar overall sensitivity. The performance of FEC codes was given in [77,78].

The coded word length is N = 64800 bits for all rates. For the 1/2 rate code, 32208 bit were encoded into the LDPC code and the remaining 196 bits were encoded into the BCH code. The I and Q bits were first interleaved. The interleaved bits were encoded into BCH code and then the LDPC code. The decoding was performed in reverse order at the receiver, where first we perform soft-decision decoding of LDPC code and then decoding of BCH code and de-interleaving. The BCH code is used to obtain error free performance as LDPC codes typically have an error floor. A BCH code with small overhead can correct for such errors and enable error free reception.

5.1.4 Optical injection locking

When light from a master laser, usually a highly coherent laser, is injected into a low coherent slave laser, the slave cavity is forced to oscillate at master frequency and following its phase. Hence the slave output will ideally be an exact replica or regenerated version of the injected master. For locking to take place, it is a necessary that the free running frequencies of both the lasers are in proximity, which is decided by a parameter called locking bandwidth and which will be discussed a little later.

Usually OIL is described by a pulling mechanism where the injected master light pulls the slave cavity to oscillate at the master frequency. This theory was first described in RF oscillators by Adler [79] in 1946 where the locking of an oscillator circuit with external RF signal injection was shown. The behaviour of pulling was first demonstrated in the optical domain by Stoven and Stier in 1966 [80] locking using two He-Ne Fabry-Perot lasers.

The locking bandwidth of the injection locking given by the following equation under steady state condition [81]:

$$\Delta\omega_{LB} = \sqrt{1 + \alpha^2} f_d \sqrt{\frac{P_{inj}}{P_{sl}}} \tag{5.1}$$

where f_d is the longitudinal mode spacing of the slave laser, α is the linewidth enhancement factor of the slave laser, P_{inj} is the injected master power and P_{sl} is the slave output power. The ratio of injected master power to the slave output power P_{inj}/P_{sl} is called the injection ratio and is an important parameter for locking bandwidth.

Locking bandwidth can be intuitively understood as the maximum allowed free running frequency difference between master and slave lasers in order to achieve locking. However, it is not necessary that stable locking can be performed even if the master and slave laser frequencies are present with in the locking bandwidth. The plot in Fig. (5.2) taken from [82] shows the optical injection ratio vs detuning frequency. The space between two solid lines where the unlocked regions share boundary is the locking bandwidth, which increases with increase in injection ratio. The region outside the locking bandwidth is
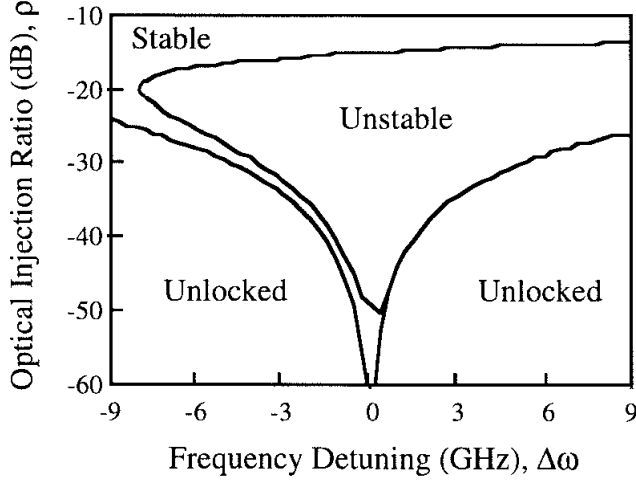
Figure 5.2: Locking characteristics of a semiconductor DFB laser [82]

the "unlocked region" where stable locking cannot be performed or a periodic locking and unlocking takes place.

The unstable region inside the locking bandwidth is called the injection locking induced pulsations (ILIP) region where slave laser shows dynamically unstable behaviour with pulsations close to relaxation frequency leading to unstable locking. Hence there exists a narrow region where stable locking can be performed. It is important that the master and slave frequencies should be very close and stable such that their frequency difference lies within the stable region especially when operated at extremely low injection ratios such as -75 dB discussed in paper (B).

In the stably locked steady state condition the locked slave output experiences a phase shift corresponding to the free running frequency difference between master and slave given by [81]

$$\Delta\phi_L = -\sin^{-1}\left(\frac{\omega_m - \omega_{sl}}{\Delta\omega_{LB}}\right) - \tan^{-1}\alpha \qquad (5.2)$$

Here $\omega_m - \omega_{sl}$ is the free running frequency difference between master and slave lasers and $\Delta\omega_{LB}$ is the locking bandwidth. The phase shift increases with decrease in locking bandwidth and at lower injection ratios this phase shift becomes large. α is a constant depends on the laser material property. The locked phase dependence property has been used in phase modulation applications where the phase is changed by modulating the drive current of the slave laser which eventually modulates the frequency of slave [83]. This equation is crucial for understanding the phase noise generated by OIL at low
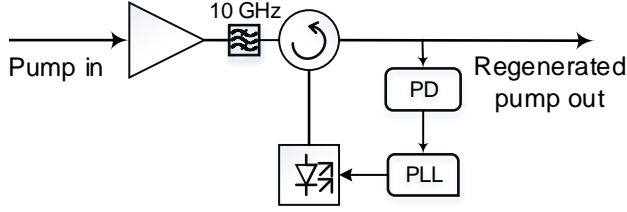
Figure 5.3: Injection locking with PLL

injection ratios, discussed in paper (B).

When it comes to practical implementation for free space communication, injection locking is challenging as the sensitivity of PSA requires pump powers to be -72 dBm or below. At this low powers, the locking bandwidth is expected to be less than 10 MHz.

Fig. 5.3 shows the injection locking set up for pump recovery in the PSA. An EDFA is used as pre amplifier to amplify the low power pump, the filter rejects some of the ASE and a PLL along with OIL is used to perform locking stably.

5.2 Challenges in implementation

There are many challenges in implementing PSA at low SNRs will be discussed here.

5.2.1 State of polarisation

The state of polarisation is critical for the practical implementations of a PSA as it will lead to unexpected problems in the process of low noise amplification. The PSA operation depend on the coherent interaction of signal and idler, therefore sensitive to polarisation, relative phase of these waves. Hence it is important that these properties are maintained constant to achieve maximum gain. There are two different stages where the polarisation must be maintained well, the copier and the PSA. The SOP of the idler generated in the copier depends on the SOP of both signal and the pump satisfying the angular momentum conservation among the four interacting photons in an isotropic medium [55].

The dependence of the SOP of the idler on SOP of signal and pump given by,

$$\frac{dU_i}{dz} = i\beta_i U_i + \frac{4i\gamma}{3}[U_P^2 U_s^* + 2U_P U_D D_S^*] \tag{5.3}$$

$$\frac{dD_i}{dz} = i\beta_i D_i + \frac{4i\gamma}{3}[D_P^2 D_s^* + 2U_P U_D U_S^*] \qquad (5.4)$$

where U_i and D_i are the field amplitudes of the left and right circular polarisation states of the idler. The same notation can be used for signal and pump waves.

Drift of the SOP of signal or the pump will result in drift of the SOP of the idler multiplied by a factor shown in Eq. (5.3) and Eq. (5.4), this will cause reduction in idler power and hence the power imbalance between signal and idler which leads to degradation of noise figure of the PSA as in Eq. (3.26). Most importantly, the different SOP's of idler and signal result in different parametric gains in the PSA as the pump is aligned to the signal polarisation, causing degradation in noise figure. As signal and idler propagate same path before the PSA, it is assumed that the SOP of the signal and idler remain in same. However, non-aligned SOPs of signal and idler result in degradation of the PSA performance.

It is possible to control them by splitting the two waves and using polarisation controllers, but that can lead to higher power loss. To avoid this problem, polarisation maintaining copier set-up is recommended.

5.2.2 Phase locked loop

Since the pump is split from signal and idler path for regeneration using injection locking, the relative phases of the waves in different paths can drift due to thermal and acoustic noise. A phase locked loop implemented to maintain the relative phase between signal, idler and pump to achieve maximum signal gain in all times. When the input signal powers into PSA are quite low, corresponding optical signal to noise ratio (OSNR) is less than 0 dB, the operation of PLL is not optimal. This is improved by filtering the signal after PSA with very narrow band filter by blocking out most of the noise and also by optimizing the PLL parameters, such as increasing sampling rate and dither frequency although doing this degrades sensitivity by a small amount.

5.2.3 Low power optical injection locking

Another challenge is stable optical injection locking at low powers as the stable locking region can be very narrow. The challenge here is to keep the free running slave frequency stable without sudden drifting because of thermal, vibrational noise in the lab or polarisation drifts in the pump which may cause OIL to unlock. SOP of the pump also can affect the locking performance as injection locking depends on SOP and it is important to maintain it stable.

5.2.4 Optimization of parametric gain

Instead of choosing a single HNLF fiber, four strained HNLF spools were chosen to reduce the Brillouin threshold and achieve best parametric again, which eventually means higher PSA gain. It is important to have high PSA gain inorder to maintain the SNR of the signal after PSA and before amplification using EDFA. As Four spools are connected by isolators between them, having a loss of 0.5 dB, reducing the noise figure of the PSA. As each spool acts as single PSA and cascaded with 3 other PSAs, acts as cascaded amplifier system with loss in between them. PSA gain of each spool is around 5 dB and overall gain is 21 dB.

As the NF of cascaded PSA depends on gain of the first spool, it is important we have maximum possible gain in the first section. This is the reason to launch pump power beyond stimulated brillouin scattering threshold value and not degrading the performance of the system.

As discussed in the injection locking section, due to low power injection locking, a locking bandwidth dependent phase noise generated in the pump wave . This results in phase noise in the pump into PSA, also increases the brillouin threshold value as we know that phase modulation of the pump can increase brillouin threshold, which eventually allows more pump power injected into PSA, resulting more PSA gain. However this also results in penalty due to in the PSA performance due to phase dependent gain. This penalty was illustrated in paper (B).

Drift in SOP of pump in copier also increases the phase noise in the pump after injection locking, resulting penalty in sensitivity.

Chapter 6

Outlook

Phase sensitive parametric amplifier have been investigated experimentally over the last two decades, still remains an interesting device seemingly far form being commercialized.

Free-space optical communications especially deep space satellites require receivers or transmitter that consume least power and occupy less space and weigh less. Certainly the current stage of the experimental PSA was far from being deployed in a real space communication satellites. However one can imagine technological developments that can make PSA simpler and cheaper to build, smaller in size and lesser weight and also consume lesser energy as the satellites have limited energy resources.

Currently PSA require pump power of the 1W, generated by high power amplifier. As one can consider having lasers of suitable characteristics with large output power without the need for high power EDFAs, where high power EDFAs consume extremely power consuming and heat dissipating. PSA is performed in a silica based HNLF spools, which are less nonlinear compared to many other platforms such as silicon nanowires , micro structured fibers or photonic crystal fibers [84] . With enough reduction of coupling losses they can become a medium of choice. The above all χ^3 media, χ^2 media also can be considered by ultizing quasi phase matching techniques. In particluar, Lithium niobate crystals (PPLN)have already been used to implement PSA, but the coupling loss of these structures is higher. This results shows modest noise figure. [85–87]

At the transmitter, the signal and idler waves needs to be amplified using booster amplifier before launching into free-space. The output powers of each wave is assumed to be half of the case where one wave considered at input (if we use EDFA instead of PSA for receiver pre-amplifier). Typically booster amplifiers operate in saturation, hence the total output power will be the same whether we use one or two waves (several 10s of Watts). Hence the transmitted

power remains same for PSA receiver or EDFA receiver and PSA is 3 dB more sensitive than EDFA for same total received power. The pump power contribution is much lower, hence its contribution after booster is assumed to be very less. There are also some implementation changes that can possibly lead to much simpler PSA. The pump was transmitted from transmitter to receiver causing penalty in the sensitivity and also adding penalty due to low power injection locking, which adds phase noise to the pump. Along with that, it might be required that, pump power needs to be transmitted at even lower power for more power efficient modulation formats. having a local pump instead of transmitting pump could avoid the penalty. By using a highly coherent laser, exactly at the same frequency as that of transmitter pump and using a faster phase locked to track the phase between the waves. However it is challenging to find laser at exactly same frequency within 100 Hz frequency difference.

Polarisation between the signal and pump waves can change when communication between moving satellites. Polarisation trackers can employed to compensate for these fluctuations as the fluctuations are slow.

Chapter 7

Summary of papers

Paper A

"High Sensitivity Receiver Demonstration Using Phase Sensitive Amplifier for Free-Space Optical Communication" Proceedings of European Conference on Optical Communications(ECOC), Paper. Tu.2.E.3, 2017.

In this paper, we demonstrated a record sensitivity of 4.5 photons per bit of using phase sensitive amplifier based receiver for free-space communication. This involves operating injection locking based pump recovery at powers as low as -62 dBm. The experiment was extended to atmospheric channel where turbulence was included in the channel by using a rotating turbulence phase plate emulating turbulence for 1 km free-space link in the lab. Results show that PSA sensitivity can be 3 dB and 1.3 dB better than EDFA when the channel is free-space without and with turbulence.

My contribution I developed the idea, performed the experiment together with Vijayan, I wrote the paper.

Paper B

The sensitivity of a PSA based receiver can be degraded mainly due to the presence of pump at the receiver input. To have a negligible penalty due to the pump, the received pump power needs to much lower than signal and idler powers. So, we need to perform injection locking below -65 dBm pump power. In this paper, we discuss the methods we have implemented for stable injection locking at powers as low as -65 dBm. A phase locked loop was employed to keep the locking stable at low powers and an EDFA pre-amplifier was used to lock at even low powers by amplifying the input. An interesting conclusion from this paper is that, using a EDFA pre-amplifier we can reduce the phase noise at the locked output rather than increasing it. We also found that the injection locking phase noise depends on the slave linewidth and that can increase with decreasing injection ratio.

We have used such a low power injection locking in PSA based receiver environment and observed a penalty of 0.4 dB relative to the case with high power pump and no injection locking, due to phase noise generated in injection locking.

My contribution I developed the idea, performed the experiment and wrote the paper.

Paper C

"Record-sensitivity Gb/s receiver for free-space applications based on phase-sensitive amplification", *Conference on Lasers and Electro-Optics (CLEO)*, pp. 1-2, 2019. (Post deadline paper).

In this paper, we implement phase sensitive amplified receiver for free-space communication, where 10 GBaud QPSK signal was encoded with DVBS2 FEC code which consists of LDPC and BCH codes was transmitted. A receiver sensitivity of error-free 1 PPB was demonstrated. The sensitivity includes received signal, idler powers together -59 dBm and -72 dBm of pump power, where SNR of the received signal is close to 0 dB. The low pump power was recovered using pre-amplified optical injection locking mechanism discussed in paper B.

My contribution I performed the experiment, including FEC implementation, Jochen processed data using DSP and wrote the paper.

Paper D

"One photon-per-bit receiver using near-noiseless phase-sensitive amplification" *Accepted for publication in Light: Science and Applications.*

This paper is an extension of the paper C, We show a black-box sensitivity of 1 PPB, where all the three waves were controlled at the transmitter, the pump was set to 12 dB below signal and idler powers and control the power of all the waves using a VOA and also introduced a free-space link. We derived a theory for capacities of all coherent receivers including PSA pre-amplified receiver.

My contribution I performed the experiment, contributed in developing the theory and wrote the paper

Paper E

Power efficient communication for high data-rate deep-space optical links, *to be submitted*.

In this paper, we demonstrate the performance of different power efficient modulation formats using PSA pre-amplified receiver. M-PPM+QPSK with higher order M values perform well at higher SNR per bit (Eb/N0) values where as smaller M values perform well at lower Eb/N0 values. A simple QPSK format outperforms all these formats at low Eb/N0 values.

My contribution I performed the theoretical calculation, experiments and wrote the DSP. Mikael worked on the DSP

References

[1] H. Hemmati, *Deep space optical communications.* John Wiley & Sons, 2006, vol. 11.

[2] D. Abraham, "Future mission trends and their implications for the deep space network," in *Space 2006*, 2006, p. 7247.

[3] W. A. Imbriale, *Large antennas of the deep space network.* John Wiley & Sons, 2005, vol. 1.

[4] K. E. Wilson, J. R. Lesh, K. Araki, and Y. Arimoto, "Overview of the Ground-to-Orbit Lasercom Demonstration," *Space Communications*, vol. 15, no. 2, pp. 89–95, 1998.

[5] J. Keller, "Optical links are key to next-generation military communications satellite," *http://mae. pennnet. com/articles/article_display. cfm? article_id= 202216*, 2004.

[6] T. Tolkeer-Nielsen and G. Oppenhauser, "In-Orbit Test Results of an Operational Inter-Satellite Link Between ARTEMIS and SPOT4, SILEX," *Proceedings of SPIE, Free-Space Laser Communication Technologies IX*, vol. 3615, pp. 31–42, 1999.

[7] H. Hemmati, *Near-earth laser communications.* CRC press, 2009.

[8] B. Smutny, R. Lange, H. Kämpfner, D. Dallmann, G. Mühlnikel, M. Reinhardt, K. Saucke, U. Sterr, B. Wandernoth, and R. Czichy, "In-orbit verification of optical inter-satellite communication links based on homodyne BPSK," in *Free-Space Laser Communication Technologies XX*, vol. 6877. International Society for Optics and Photonics, 2008, p. 687702.

[9] D. M. Boroson, B. S. Robinson, D. V. Murphy, D. A. Burianek, F. Khatri, J. M. Kovalik, Z. Sodnik, and D. M. Cornwell, "Overview and results of the lunar laser communication demonstration," in *Free-Space Laser Communication and Atmospheric Propagation XXVI*, vol. 8971. International Society for Optics and Photonics, 2014, p. 89710S.

[10] A. Biswas, "NASA's Deep Space Optical Communications–an Update," in *Applications of Lasers for Sensing and Free Space Communications*. Optical Society of America, 2019, pp. LTh1B–1.

[11] D. M. Cornwell, "Nasa's optical communications program for 2017 and beyond," in *2017 IEEE International Conference on Space Optical Systems and Applications (ICSOS)*. IEEE, 2017, pp. 10–14.

[12] A. Seas, B. Robinson, T. Shih, F. Khatri, and M. Brumfield, "Optical communications systems for NASA's human space flight missions," in *International Conference on Space Optics?ICSO 2018*, vol. 11180. International Society for Optics and Photonics, 2019, p. 111800H.

[13] Z. Sodnik, H. Smit, M. Sans, I. Zayer, M. Lanucara, I. Montilla, and A. Alonso, "LLCD operations using the Lunar Lasercom OGS Terminal," in *Free-Space Laser Communication and Atmospheric Propagation XXVI*, vol. 8971. International Society for Optics and Photonics, 2014, p. 89710W.

[14] D. J. Geisler, T. M. Yarnall, M. L. Stevens, C. M. Schieler, B. S. Robinson, and S. A. Hamilton, "Multi-aperture digital coherent combining for free-space optical communication receivers," *Optics Express*, vol. 24, no. 12, pp. 12 661–12 671, 2016.

[15] D. J. Geisler, C. M. Schieler, T. M. Yarnall, M. L. Stevens, B. S. Robinson, and S. A. Hamilton, "Demonstration of a variable data-rate free-space optical communication architecture using efficient coherent techniques," *Optical Engineering*, vol. 55, no. 11, p. 111605, 2016.

[16] M. Karlsson and E. Agrell, "Which is the most power-efficient modulation format in optical links?" *Optics express*, vol. 17, no. 13, pp. 10 814–10 819, 2009.

[17] E. Agrell and M. Karlsson, "Power-efficient modulation formats in coherent transmission systems," *Journal of Lightwave Technology*, vol. 27, no. 22, pp. 5115–5126, 2009.

[18] A. Ludwig, M.-L. Schulz, P. Schindler, S. Wolf, C. Koos, W. Freude, and J. Leuthold, "Stacked modulation formats enabling highest-sensitivity optical free-space links," *Optics express*, vol. 23, no. 17, pp. 21 942–21 957, 2015.

[19] C. Gobby, Z. Yuan, and A. Shields, "Quantum key distribution over 122 km of standard telecom fiber," *Applied Physics Letters*, vol. 84, no. 19, pp. 3762–3764, 2004.

[20] N. Bertone, R. Biasi, and B. Dion, "Overview of photon counting detectors based on cmos processed single photon avalanche diodes (spad), ingaas apds, and novel hybrid (tube+ apd) detectors," in *Semiconductor Photodetectors II*, vol. 5726. International Society for Optics and Photonics, 2005, pp. 153–164.

[21] M. D. Eisaman, J. Fan, A. Migdall, and S. V. Polyakov, "Invited review article: Single-photon sources and detectors," *Review of scientific instruments*, vol. 82, no. 7, p. 071101, 2011.

[22] C. M. Caves, "Quantum limits on noise in linear amplifiers," *Physical Review D*, vol. 26, no. 8, p. 1817, 1982.

[23] R. Slavík, F. Parmigiani, J. Kakande, C. Lundström, M. Sjödin, P. A. Andrekson, R. Weerasuriya, S. Sygletos, A. D. Ellis, L. Grüner-Nielsen *et al.*, "All-optical phase and amplitude regenerator for next-generation telecommunications systems," *Nature Photonics*, vol. 4, no. 10, pp. 690–695, 2010.

[24] Z. Tong, C. Lundström, P. Andrekson, C. McKinstrie, M. Karlsson, D. Blessing, E. Tipsuwannakul, B. Puttnam, H. Toda, and L. Grüner-Nielsen, "Towards ultrasensitive optical links enabled by low-noise phase-sensitive amplifiers," *Nature photonics*, vol. 5, no. 7, p. 430, 2011.

[25] J. Hansryd, P. A. Andrekson, M. Westlund, J. Li, and P.-O. Hedekvist, "Fiber-based optical parametric amplifiers and their applications," *IEEE Journal of Selected Topics in Quantum Electronics*, vol. 8, no. 3, pp. 506–520, 2002.

[26] C. Lundström, E. Myslivets, A. O. Wiberg, N. Alic, S. Radic, M. Karsson, and P. A. Andrekson, "Tension-optimized highly nonlinear fiber for parametric applications," in *European Conference and Exhibition on Optical Communication*. Optical Society of America, 2012, pp. We–1.

[27] S. Arnon, J. Barry, G. Karagiannidis, R. Schober, and M. Uysal, *Advanced optical wireless communication systems*. Cambridge university press, 2012.

[28] A. K. Majumdar, *Advanced free space optics (FSO): A systems approach*. Springer, 2014, vol. 186.

[29] R. Elliot, "Ieee standard definitions of terms for antennas," *IEEE Transactions on Antennas and Propagation*, vol. 31, no. 6, pp. 1–29, 1983.

[30] A. Ishimaru, *Wave propagation and scattering in random media*. John Wiley & Sons, 1999, vol. 12.

[31] L. C. Andrews and R. L. Phillips, *Laser beam propagation through random media.* SPIE press Bellingham, WA, 2005, vol. 152.

[32] A. K. Majumdar and J. C. Ricklin, *Free-space laser communications: principles and advances.* Springer Science & Business Media, 2010, vol. 2.

[33] S. M. Ebstein, "Pseudo-random phase plates," in *High-Resolution Wavefront Control: Methods, Devices, and Applications III*, vol. 4493. International Society for Optics and Photonics, 2002, pp. 150–155.

[34] Y. Ren, H. Huang, G. Xie, N. Ahmed, Y. Yan, B. I. Erkmen, N. Chandrasekaran, M. P. Lavery, N. K. Steinhoff, M. Tur *et al.*, "Atmospheric turbulence effects on the performance of a free space optical link employing orbital angular momentum multiplexing," *Optics letters*, vol. 38, no. 20, pp. 4062–4065, 2013.

[35] P. Polynkin, A. Peleg, L. Klein, T. Rhoadarmer, and J. Moloney, "Optimized multiemitter beams for free-space optical communications through turbulent atmosphere," *Optics letters*, vol. 32, no. 8, pp. 885–887, 2007.

[36] R. Stolen, "Phase-matched-stimulated four-photon mixing in silica-fiber waveguides," *IEEE Journal of Quantum Electronics*, vol. 11, no. 3, pp. 100–103, 1975.

[37] R. Stolen and J. Bjorkholm, "Parametric amplification and frequency conversion in optical fibers," *IEEE Journal of Quantum Electronics*, vol. 18, no. 7, pp. 1062–1072, 1982.

[38] J. Armstrong, N. Bloembergen, J. Ducuing, and P. Pershan, "Interactions between light waves in a nonlinear dielectric," *Physical review*, vol. 127, no. 6, p. 1918, 1962.

[39] N. M. Kroll, "Parametric amplification in spatially extended media and application to the design of tuneable oscillators at optical frequencies," *Physical Review*, vol. 127, no. 4, p. 1207, 1962.

[40] R. Gadonas, A. Marcinkevičius, A. Piskarskas, V. Smilgevičius, and A. Stabinis, "Travelling wave optical parametric generator pumped by a conical beam," *Optics communications*, vol. 146, no. 1-6, pp. 253–256, 1998.

[41] C. M. Caves, "Quantum limits on noise in linear amplifiers," *Phys. Rev. D*, vol. 26, pp. 1817–1839, Oct 1982.

[42] J. A. Levenson, I. Abram, T. Rivera, and P. Grangier, "Reduction of quantum noise in optical parametric amplification," *JOSA B*, vol. 10, no. 11, pp. 2233–2238, 1993.

[43] W. Imajuku, A. Takada, and Y. Yamabayashi, "Low-noise amplification under the 3 db noise figure in high-gain phase-sensitive fibre amplifier," *Electronics Letters*, vol. 35, no. 22, pp. 1954–1955, 1999.

[44] C. McKinstrie and S. Radic, "Phase-sensitive amplification in a fiber," *Optics express*, vol. 12, no. 20, pp. 4973–4979, 2004.

[45] S. L. Olsson, H. Eliasson, E. Astra, M. Karlsson, and P. A. Andrekson, "Long-haul optical transmission link using low-noise phase-sensitive amplifiers," *Nature communications*, vol. 9, no. 1, p. 2513, 2018.

[46] G. P. Agrawal, "Nonlinear fiber optics," in *Nonlinear Science at the Dawn of the 21st Century*.   Springer, 2000, pp. 195–211.

[47] T. Schneider, *Nonlinear optics in telecommunications*.   Springer Science & Business Media, 2013.

[48] K. Hill, D. Johnson, B. Kawasaki, and R. MacDonald, "cw three-wave mixing in single-mode optical fibers," *Journal of Applied Physics*, vol. 49, no. 10, pp. 5098–5106, 1978.

[49] N. Shibata, R. Braun, and R. Waarts, "Phase-mismatch dependence of efficiency of wave generation through four-wave mixing in a single-mode optical fiber," *IEEE Journal of Quantum Electronics*, vol. 23, no. 7, pp. 1205–1210, 1987.

[50] Y. Yamamoto and H. Haus, "Preparation, measurement and information capacity of optical quantum states," *Reviews of Modern Physics*, vol. 58, no. 4, p. 1001, 1986.

[51] K. Kikuchi, "Fundamentals of coherent optical fiber communications," *Journal of Lightwave Technology*, vol. 34, no. 1, pp. 157–179, 2015.

[52] C. J. McKinstrie, S. Radic, and M. Raymer, "Quantum noise properties of parametric amplifiers driven by two pump waves," *Optics Express*, vol. 12, no. 21, pp. 5037–5066, 2004.

[53] K. Kikuchi and S. Tsukamoto, "Evaluation of sensitivity of the digital coherent receiver," *Journal of Lightwave Technology*, vol. 26, no. 13, pp. 1817–1822, 2008.

[54] E. Ip, A. P. T. Lau, D. J. Barros, and J. M. Kahn, "Coherent detection in optical fiber systems," *Optics express*, vol. 16, no. 2, pp. 753–791, 2008.

[55] G. P. Agrawal, *Fiber-optic communication systems*.   John Wiley & Sons, 2012, vol. 222.

[56] M. Y. Leong, G. Jacobsen, S. Popov, and S. Sergeyev, "Receiver sensitivity in optical and microwave, heterodyne and homodyne systems," *Journal of optical communications*, vol. 35, no. 3, pp. 221–229, 2014.

[57] J. Katz, "The 2.5 bit/detected photon demonstration program: Phase 2 and 3 experimental results," 1982.

[58] D. J. Geisler, T. M. Yarnall, W. E. Keicher, M. L. Stevens, A. M. Fletcher, R. R. Parenti, D. O. Caplan, and S. A. Hamilton, "Demonstration of 2.1 photon-per-bit sensitivity for BPSK at 9.94-gb/s with rate-1/2 FEC," in *2013 Optical Fiber Communication Conference and Exposition and the National Fiber Optic Engineers Conference (OFC/NFOEC)*. IEEE, 2013, pp. 1–3.

[59] D. Yoon, K. Cho, and J. Lee, "Bit error probability of M-ary quadrature amplitude modulation," in *Vehicular Technology Conference Fall 2000. IEEE VTS Fall VTC2000. 52nd Vehicular Technology Conference (Cat. No. 00CH37152)*, vol. 5. IEEE, 2000, pp. 2422–2427.

[60] M. Karlsson and E. Agrell, "Multilevel pulse-position modulation for optical power-efficient communication," *Optics express*, vol. 19, no. 26, pp. B799–B804, 2011.

[61] X. Liu, S. Chandrasekhar, T. Wood, R. Tkach, E. Burrows, and P. Winzer, "Demonstration of 2.7-ppb receiver sensitivity using PDM-QPSK with 4-PPM and unrepeatered transmission over a single 370-km unamplified ultra-large-area fiber span," in *2011 37th European Conference and Exhibition on Optical Communication*. IEEE, 2011, pp. 1–3.

[62] C. E. Shannon, "A mathematical theory of communication," *ACM SIGMOBILE mobile computing and communications review*, vol. 5, no. 1, pp. 3–55, 2001.

[63] J. P. Gordon, "Quantum effects in communications systems," *Proceedings of the IRE*, vol. 50, no. 9, pp. 1898–1908, 1962.

[64] H. Hemmati, K. Birnbaum, W. Farr, S. Turyshev, and A. Biswas, "Combined laser communications and laser ranging transponder for Moon and Mars," in *Free-Space Laser Communication Technologies XXI*, vol. 7199. International Society for Optics and Photonics, 2009, p. 71990N.

[65] Y. Yang, C. Geng, F. Li, G. Huang, and X. Li, "Multi-aperture all-fiber active coherent beam combining for free-space optical communication receivers," *Optics Express*, vol. 25, no. 22, pp. 27519–27532, 2017.

[66] P. Hopman, P. Boettcher, L. M. Candell, J. Glettler, R. Shoup, and G. Zogbi, "An end-to-end demonstration of a receiver array based free-space photon counting communications link," in *Free-Space Laser Communications VI*, vol. 6304. International Society for Optics and Photonics, 2006, p. 63040H.

[67] M. Willis, A. Kerman, M. Grein, J. Kansky, B. Romkey, E. Dauler, D. Rosenberg, B. Robinson, D. Murphy, and D. Boroson, "Performance of a multimode photon-counting optical receiver for the NASA Lunar Laser Communications demonstration," in *International Conference on Space Optical Systems and Applications (ICSOS)*, 2012.

[68] M. Stevens, D. Caplan, B. Robinson, D. Boroson, and A. Kachelmyer, "Optical homodyne PSK demonstration of 1.5 photons per bit at 156 mbps with rate-1/2 turbo coding," *Optics Express*, vol. 16, no. 14, pp. 10 412–10 420, 2008.

[69] X. Liu, T. Wood, R. Tkach, and S. Chandrasekhar, "Demonstration of record sensitivity in an optically pre-amplified receiver by combining PDM-QPSK and 16-PPM with pilot-assisted digital coherent detection," in *National Fiber Optic Engineers Conference*. Optical Society of America, 2011, p. PDPB1.

[70] D. O. Caplan, B. S. Robinson, R. J. Murphy, and M. L. Stevens, "Demonstration of 2.5-gslot/s optically-preamplified M-PPM with 4 photons/bit receiver sensitivity," in *Optical Fiber Communication Conference*. Optical Society of America, 2005, p. PDP32.

[71] D. Lavery, S. Liu, Y. Jeong, J. Nilsson, P. Petropoulos, P. Bayvel, and S. J. Savory, "Realizing high sensitivity at 40 Gbit/s and 100 Gbit/s," in *OFC/NFOEC*. IEEE, 2012, pp. 1–3.

[72] T. Mizuochi, Y. Miyata, T. Kobayashi, K. Ouchi, K. Kuno, K. Kubo, K. Shimizu, H. Tagami, H. Yoshida, H. Fujita *et al.*, "Forward error correction based on block turbo code with 3-bit soft decision for 10-gb/s optical communication systems," *IEEE Journal of Selected Topics in Quantum Electronics*, vol. 10, no. 2, pp. 376–386, 2004.

[73] S. L. Olsson, B. Corcoran, C. Lundström, T. A. Eriksson, M. Karlsson, and P. A. Andrekson, "Phase-sensitive amplified transmission links for improved sensitivity and nonlinearity tolerance," *Journal of Lightwave Technology*, vol. 33, no. 3, pp. 710–721, 2014.

[74] H. Eliasson, K. Vijayan, B. Foo, S. L. Olsson, E. Astra, M. Karlsson, and P. A. Andrekson, "Phase-sensitive amplifier link with distributed Raman amplification," *Optics Express*, vol. 26, no. 16, pp. 19 854–19 863, 2018.

[75] Y. Okamura, K. Kondo, S. Seki, Y. Ohmichi, M. Koga, and A. Takada, "Frequency nondegenerate optical parametric phase-sensitive amplifier repeater by using recovered pump carrier generated from phase-conjugated twin waves," in *Optical Fiber Communications Conference and Exhibition (OFC), 2016*. IEEE, 2016, pp. 1–3.

[76] S. J. Savory, "Digital coherent optical receivers: Algorithms and subsystems," *IEEE Journal of selected topics in quantum electronics*, vol. 16, no. 5, pp. 1164–1179, 2010.

[77] M. Eroz, F.-W. Sun, and L.-N. Lee, "DVB-S2 low density parity check codes with near Shannon limit performance," *International Journal of Satellite Communications and Networking*, vol. 22, no. 3, pp. 269–279, 2004.

[78] A. Morello and V. Mignone, "DVB-S2: The second generation standard for satellite broad-band services," *Proceedings of the IEEE*, vol. 94, no. 1, pp. 210–227, 2006.

[79] R. Adler, "A study of locking phenomena in oscillators," *Proceedings of the IRE*, vol. 34, no. 6, pp. 351–357, 1946.

[80] H. Stover and W. Steier, "Locking of laser oscillators by light injection," *applied physics letters*, vol. 8, no. 4, pp. 91–93, 1966.

[81] F. Mogensen, H. Olesen, and G. Jacobsen, "Locking conditions and stability properties for a semiconductor laser with external light injection," *IEEE Journal of Quantum Electronics*, vol. 21, no. 7, pp. 784–793, 1985.

[82] J. Yao, "Microwave photonics," *Journal of Lightwave Technology*, vol. 27, no. 3, pp. 314–335, 2009.

[83] S. Kobayashi and T. Kimura, "Optical phase modulation in an injection locked algaas semiconductor laser," *Electronics Letters*, vol. 18, no. 5, pp. 210–211, 1982.

[84] P. Russell, "Photonic crystal fibers," *Science*, vol. 299, no. 5605, pp. 358–362, 2003.

[85] K. J. Lee, F. Parmigiani, S. Liu, J. Kakande, P. Petropoulos, K. Gallo, and D. Richardson, "Phase sensitive amplification based on quadratic cascading in a periodically poled lithium niobate waveguide," *Optics Express*, vol. 17, no. 22, pp. 20 393–20 400, 2009.

[86] B. J. Puttnam, D. Mazroa, S. Shinada, and N. Wada, "Large phase sensitive gain in periodically poled lithium niobate with high pump power," *IEEE Photonics Technology Letters*, vol. 23, no. 7, pp. 426–428, 2011.

[87] ——, "Phase-squeezing properties of non-degenerate PSAs using PPLN waveguides," *Optics express*, vol. 19, no. 26, pp. B131–B139, 2011.

Included papers A–E

Paper A

R. Kakarla, K. Vijayan, A. Lorences-Riesgo, P. A Andrekson, "High Sensitivity Receiver Demonstration Using Phase Sensitive Amplifier for Free-Space Optical Communication", *Proceedings of European Conference on Optical Communications(ECOC)*, Paper. Tu.2.E.3, 2017.

Paper B

R. Kakarla, J. Schröder, and P.A. Andrekson, "Optical injection locking at sub nano-Watt powers", *Optics Letters*. vol. 43, no. 23, pp. 5769-5772, 2016.

Paper C

R. Kakarla, J. Schröder, and P.A. Andrekson, "Record-sensitivity Gb/s receiver for free-space applications based on phase-sensitive amplification", *Conference on Lasers and Electro-Optics (CLEO)*, pp. 1-2, 2019. (Post deadline paper).

Paper D

Paper E

R. Kakarla, J. Schröder, and P.A. Andrekson, "Power efficient communication for high data-rate deep-space optical links", *To be submitted.*